National Aeronautics and Space Administration

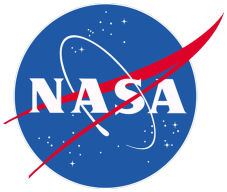

Algorithm Theoretical Basis Document (ATBD)

NASA Global Precipitation Measurement (GPM) Integrated Multi-satellitE Retrievals for GPM (IMERG) Version 07

Prepared for:

Global Precipitation Measurement (GPM)
National Aeronautics and Space Administration (NASA)

Prepared by:

George J. Huffman
NASA/GSFC
NASA/GSFC Code 612
Greenbelt, MD 20771

and David T. Bolvin, Robert Joyce, Eric J. Nelkin, Jackson Tan, Dan Braithwaite, Kuolin Hsu, Owen A. Kelley, Phu Nguyen, Soroosh Sorooshian, Daniel C. Watters, B. Jason West, Pingping Xie

12 July 2023

TABLE OF CONTENTS

LIST OF FIGURES

LIST OF TABLES

1 INTRODUCTION

1.1 Objective

This document describes the algorithm and processing sequence for the Integrated Multi-satellitE Retrievals for the Global Precipitation Measurement (GPM) mission (IMERG). This algorithm is intended to intercalibrate, merge, and interpolate "all" satellite microwave precipitation estimates, together with microwave-calibrated infrared (IR) satellite estimates, precipitation gauge analyses, and potentially other precipitation estimators at fine time and space scales for the Tropical Rainfall Measuring Mission (TRMM) and GPM eras over the entire globe. To date, TRMM and GPM together constitute the Precipitation Measurement Missions (PMM) project. The system is run several times for each observation time, first giving a quick estimate and successively providing better estimates as more data arrive. The final step uses monthly gauge data to create research-level products. Background information and references are provided to describe the context and the relation to other similar missions. Issues involved in understanding the accuracies obtained from the calculations are discussed. Throughout, the current Version 07 product is described, together with options and planned improvements that might be instituted in future version(s) depending on maturity and project constraints.

1.2 Revision History

Version	*Date*	*Lead Author*	*Description*
1.0	30 November 2010	G. Huffman	Initial version
2.0	30 November 2011	G. Huffman	Second delivery version
3.0	30 November 2012	G. Huffman	Third delivery version
3.1	12 July 2013	G. Huffman	Document Prob. Liq. Precip. Type
4	30 September 2013	G. Huffman	Fourth delivery version
4.1	16 December 2013	G. Huffman	At-launch modifications
4.2	20 December 2013	G. Huffman	Edits; add overpass diagram
4.3	22 July 2014	G. Huffman	Edits for post-launch information
4.4	15 September 2014	G. Huffman	Change to single snapshot each half hour
4.5	16 November 2015	G. Huffman	Version and Run file naming, current status, input satellite dates
4.6	14 March 2017	G. Huffman	Initial upgrade to GPM V05
5	9 November 2017	G. Huffman	Upgrade to IMERG V05
5.1	10 November 2017	G. Huffman	No GPROF-TMI; trimmed MHS, ATMS swaths
5.2	1 February 2018	G. Huffman	
6	13 March 2019	G. Huffman	Upgrade to IMERG V06
6.1	18 March 2019	G. Huffman	Expand on calibration at start-ups
6.2	8 October 2019	G. Huffman	Note Early, Late not cal. to Final; shift of ERA-Interim to ERA5 for Final PLPP field
6.3	3 January 2020	G. Huffman	Correct supply of input data to retrospective Early and Late
7.0	10 July 2023	G. Huffman	Upgrade to IMERG V07

2 OBSERVING SYSTEMS

Historically and for the foreseeable future, passive microwave (PMW) sensors provide the lion's share of relatively accurate satellite-based precipitation estimates, and these are only available from low-Earth-orbit (leo) platforms. IMERG is designed to compensate for the limited sampling available from single leo-satellites by using as many leo-satellites as possible, and then augmenting with geosynchronous-Earth-orbit (geo) infrared (IR) estimates. This happens in two ways. First, the leo-PMW data are morphed (quasi-Lagrangian linear interpolation following the estimated precipitation-feature motion based on several precipitation-related data fields in reanalysis and numerical model data). Second, geo-IR precipitation estimates are included using a Kalman filter when the leo-PMW are too sparse. Additionally, precipitation gauge analyses are used to provide crucial regionalization and bias correction to the satellite estimates. None of the leo-satellites, except the GPM Core Observatory (GPM-CO) satellite, are under GPM direction. Therefore, IMERG uses as many satellites of opportunity ("constellation" satellites) as possible in a very flexible framework. Table 1 gives a listing of the current and planned data sources, and the date spans of useful operation. Note that we plan to provide a continuous record from the beginning of TRMM. In all cases except the geo-IR the input satellite data are accessed as Level 2 (scan-pixel) precipitation.

2.1 Core Satellites

The TRMM satellite and GPM Core Observatory serve as both a calibrator and an evaluation tool for all the PMW- and IR-based precipitation products integrated in IMERG in their respective eras, since they provide matchups with all other PMW-equipped leo-satellites and IR-equipped geo-satellites. [Note that all of the intercalibrated PMW data are used to calibrate the IR estimates.] Both the TRMM and GPM satellites provide multi-channel, dual-polarization PMW sensors and active scanning radars. Three critical improvements in GPM are that 1) the orbital inclination has been increased from 35° to 65°, affording coverage of important additional climate zones; 2) the radar has been upgraded to two frequencies, adding sensitivity to light precipitation; and 3) "high-frequency" channels (165.5 and 183.3 GHz) have been included in the GPM Microwave Imager (GMI), which provide key information for sensing light and solid precipitation. The higher inclination of the GPM orbit reduces the radiometer and radar sampling compared to TRMM in the latitude band covered by TRMM. It should be noted that the radar estimates from both satellites are used for calibration and evaluation, and are not directly inserted into any of the IMERG estimates.

2.2 Microwave Constellation

The constellation of PMW satellites (Figure 1) is largely composed of satellites of opportunity. That is, with the exception of the GPM-CO and the TRMM satellite, their orbital characteristics, operations, channel selections, and data policies are outside the purview of the NASA PMM program. The imager channels are considered best for low- and mid-latitude use, particularly over ocean, while the sounding channels maintain some skill in cold and frozen-surface conditions.

2.3 IR Constellation

Although three different organizations control the geo-IR satellites, long-standing international agreements ensure coordination of orbits and mutual aid in the event of an unexpected satellite failure. The basic requirement is for full-disk images every three hours at the major synoptic times

(00, 03, …, 21 UTC). All satellite operators provide a great deal of imagery beyond that, although piecing it together into a unified, consistent field can be somewhat challenging. These data are accessed as brightness temperatures (Tb) in the merged format developed at National Oceanic and Atmospheric Administration Climate Prediction Center (NOAA/CPC), who also routinely assemble the dataset. Note that the long-term archive is located at https://disc.gsfc.nasa.gov/datasets/GPM_MERGIR_1/summary.

Table 1. List of current and planned contributing data sets for IMERG, broken out by sensor type. Data sets with start dates of Jan 98 extend before that time, but these prior data are not used in IMERG. Square brackets ([ ]) indicate an estimated date. The geosynchronous IR data are processed into merged files at NOAA/CPC. All data are at Level 2 (scan/pixel) except for the precipitation gauge analyses and IR data, which are at Level 3 (gridded). PPS maintains a list of anomalies in the microwave constellation sensors at https://gpmweb2https.pps.eosdis.nasa.gov/tsdis/AB/docs/gpm_anomalous.html. Gray-shaded entries are not currently used, but are stated for possible future use.

Merged Radar – Passive Microwave Imager Products	
Product	*Period of Record*
GPM DPR-GMI	Apr 14 - [Dec 29]
TRMM PR-TMI	Jan 98 - Sep 14

Conically-Scanning Passive Microwave Imagers and Imager/Sounders	
Sensor	*Period of Record*
Aqua AMSR-E	Jun 02 - Oct 11
DMSP F13 SSMI	Jan 98 - Nov 09
DMSP F14 SSMI	Jan 98 - Aug 08
DMSP F15 SSMI	Feb 00 - Aug 06
DMSP F16 SSMIS	Nov 05 - [Dec 24]
DMSP F17 SSMIS	Mar 08 - [Dec 25]
DMSP F18 SSMIS	Mar 10 - [Mar 26]
DMSP F19 SSMIS	Dec 14 – Feb 16
GCOMW1 AMSR2	Jul 12 - [May 26]
GOSAT-3 AMSR3	[Feb 24] - [Jan 32]
GPM GMI	Mar 14 - [Dec 29]
METOP-SG B1 MWI	[Jan 24] – [Dec 34]
METOP-SG B2 MWI	[Jan 29] – [Dec 39]
METOP-SG B3 MWI	[Jan 36] – [Dec 46]
TRMM TMI	Jan 98 – Apr 15
WSF-M 1 MIS	[Jan 24 – Jan 30]
WSF-M 2 MIS	[Jan 28 – Jan 34]

Table 1, continued.

Cross-Track-Scanning Passive Microwave Sounders	
Sensor	*Period of Record*
JPSS-3 ATMS **	[Jan 26] - [Jan 32]
JPSS-4 ATMS **	[Jan 31] - [Jan 37]
METOP-2/A MHS **	Dec 06 - Jan 20
METOP-1/B MHS **	Apr 13 - [Aug 26]
METOP-3/C MHS	Nov 19 - [Apr 27]
METOP-SG A1 MWS	[Jan 22] – [Dec 32]
METOP-SG A2 MWS	[Jan 29] – [Dec 39]
METOP-SG A3 MWS	[Jan 36] – [Dec 46]
M-T SAPHIR *	Oct 11 - Mar 22
NOAA-15 AMSU **	Jan 00 - Sep 10
NOAA-16 AMSU **	Oct 00 - Apr 10
NOAA-17 AMSU **	Jun 02 - Dec 09
NOAA-18 MHS **	May 05 – Oct 18
NOAA-19 MHS **	Feb 09 - [Dec 23]
NOAA-20 ATMS **	Nov 17 - [Aug 24]
NOAA-21 ATMS **	Jun 23 - [Jan 30]
SNPP ATMS **	Dec 11 - [Dec 24]

* Parts of the SAPHIR record suffer drop-outs. As well, the PRPS estimates do not provide estimates for the 5 footprints at each swath edge. SAPHIR is not used in V07 IMERG to allow additional retrieval development to provide more consistent spatial patterns with other PMW retrievals.

** The V07 GPROF estimates for AMSU, ATMS, and MHS do not provide estimates for the 5, 8, and 5 footprints (respectively) at each swath edge.

Geosynchronous Infrared Imagers		
Satellite	*Sub-sat. Lon.*	*Agency*
EWS-G1 (old GOES-13)	161°E	U.S. DoD/NOAA
GMS, MTSat, Himawari series	140°E	JMA
GOES-E series	75°W	NESDIS
GOES-W series	135°W	NESDIS
Meteosat prime series	0°E	EUMETSAT
Meteosat repositioned series	63°E, from Jul 98 41°E, from Oct 16	EUMETSAT

Precipitation Gauge Analyses		
Analysis	*Period of Record*	*Institution*
Full Version 2022	Jan 98 – Dec 20	DWD/GPCC

Monitoring Version 2022	Jan 21 - ongoing	DWD/GPCC

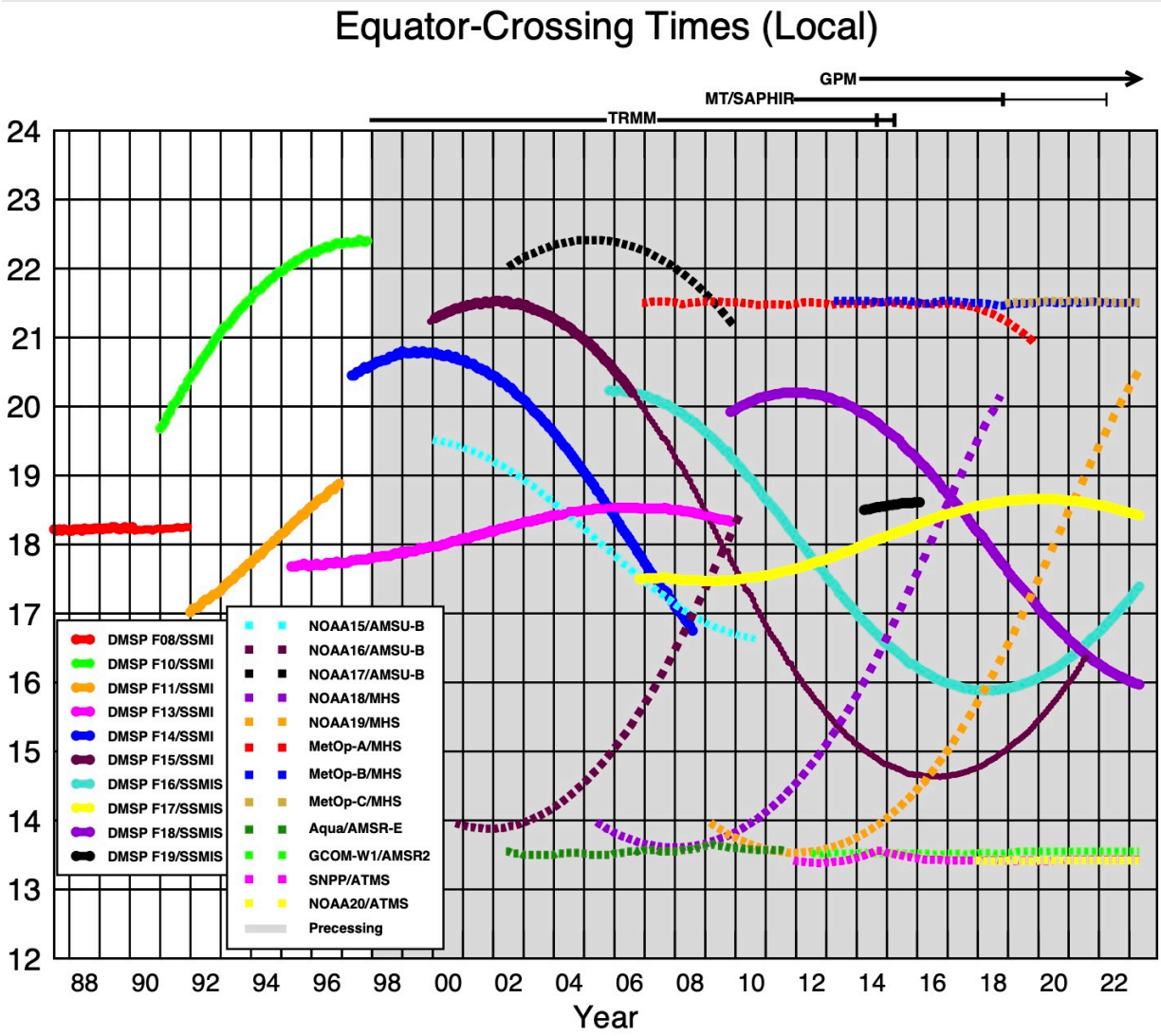

Ascending passes (F08 descending); satellites depicted above graph precess throughout the day.
Image by Eric Nelkin (SSAI), 13 June 2023, NASA/Goddard Space Flight Center, Greenbelt, MD.
https://gpm.nasa.gov/resources/images/gpm-constellation-overpass-times

Figure 1. PMW sensor Equator-crossing times for 12-24 Local Time (LT; 00-12 LT is the same) for the modern PMW sensor era. These are all ascending passes, except F08 is descending. Shading indicates that the precessing orbits of TRMM, Megha-Tropiques, and GPM cover all times of day. [Image by Eric Nelkin (SSAI; GSFC), 13 June 2023; https://gpm.nasa.gov/resources/images/gpm-constellation-overpass-times holds the current version.]

2.4 Additional Satellites

Recent work by CPC and subsequently Univ. of Arizona (Ehsani et al. 2021) has shown some skill in using IR data from the Advanced Very High Resolution Radiometer (AVHRR) from low-orbit satellites for estimating precipitation at high latitudes. Adding any of these data is probably beyond the scope of IMERG at this juncture.

2.5 Precipitation Gauges

Work in GPCP and TRMM has shown that incorporating a uniform precipitation gauge analysis is important for controlling the bias that typifies satellite precipitation estimates. These projects show that even monthly gauge analyses produce significant improvements, at least for some regions in some seasons. Recent work at CPC shows substantial improvements in the bias correction using daily gauge analysis for regions in which there is a sufficient number of gauges. The Climate Hazards center IMErg with Stations (CHIMES; Funk et al. 2022) scheme has shown good skill combining IMERG with pentad gauge data, and might represent the most promising avenue for such work globally.

The Deutscher Wetterdienst (DWD) Global Precipitation Climatology Centre (GPCC) was established in 1989 to provide high-quality precipitation analyses over land based on conventional precipitation gauges. We use two GPCC products, the V2022 Full Data Analysis for the majority of the time (currently 1998-2020), and the V2022 Monitoring Product from 2020 to the -present.

The Monitoring Product is posted about two months after the month of observation (see Becker et al. 2013; Schneider et al. 2014, 2018) and is based on SYNOP and monthly CLIMAT reports received in near real-time via GTS from ~7,000–9,000 stations world-wide reported in the following sources:

- monthly precipitation totals accumulated at GPCC from the SYNOP reports received at DWD, Offenbach, Germany,
- monthly precipitation totals accumulated at NOAA/CPC from the SYNOP reports received at NOAA, Washington D.C.,
- monthly precipitation totals from CLIMAT reports received at DWD, Offenbach, Germany,
- monthly precipitation totals from CLIMAT reports received at the UK Met. Office (UKMO), Exeter, UK, and
- monthly precipitation totals from CLIMAT reports received at Japan Meteorological Agency (JMA), Tokyo, Japan.

GPCC's Full Data Analysis is based on a database that covers the period 1901 up to 2020 (current V2022 released in August 2022). Compared to the Monitoring Product, the Full Data Analysis includes additional data acquired from global data collections such as GHCN, FAO, CRU; data sets from the National Meteorological and/or Hydrological Services of about 190 countries of the world; and some data from GEWEX-related projects.

For both products, if data are available from more than one source for a station, an "optimum" value – according to the quality of the different data sources – is selected for the precipitation analysis. The selected precipitation data undergo an automatic pre-screening, and subsequently the data flagged as questionable are interactively reviewed by an expert. Based on the remaining quality-controlled station data, the (monthly) anomalies from the background climatology are computed at each station, interpolated using the SPHEREMAP objective analysis, and added to

the background climatology to create the month's analysis. Note that anomalies that are "too distant" from any stations are set to zero to prevent unrealistic influence across vast distances.

CPC collects daily precipitation gauge data from ~16,000 stations around the world through the GTS, and from enhanced national networks over the U.S., Mexico, and a few other countries. They analyze global daily precipitation on a near-real-time basis by interpolating quality-controlled station reports. Note that the "day" in this analysis is defined region by region, not at a uniform UTC time. Alternatively, The Climate Hazards Center (CHC) at University of California Santa Barbara curates an extensive archive of stations referred to as the CHC Station Climatology Database (CSCD; Funk et al. 2022) that provides a similar global database, although CHC advocates for using multi-day accumulations of data at stations to create more stable statistics. These data are the basis for the daily satellite-gauge option in Sec. 3.15.4.

Precipitation gauges suffer a variety of errors in collecting precipitation, including evaporation, splashing, side wetting, and wind effects, with all these error sources creating a low bias for most gauge configurations. The wind effects occur because the air has to flow around the opening of the gauge and hydrometeors tend to follow the air flow. This effect is more pronounced for hydrometeors that fall the slowly, namely drizzle and snowflakes. Undercatch ranges from 5% in heavy rain and higher in other conditions, and depends on the design of the gauge (Legates 1987; Sevruk 1989). Legates and Willmott (1990) monthly climatological undercatch corrections are applied, except a monthly climatology based on the Fuchs et al. (2001) analysis is applied over Eurasia north of 45°N.

3 ALGORITHM DESCRIPTION

Given the available diverse, changing, uncoordinated set of input precipitation estimates with various periods of record, regions of coverage, and sensor-specific strengths and limitations, we seek to compute the longest, most detailed record of "global" precipitation. To do this, we combine the input estimates into a "best" data set. Although we wish to maintain reasonable homogeneity in the input datasets, for example by using consistently processed archives for each sensor and undertaking multiple inter-calibrations, we are not striving to compute a Climate Data Record dataset (CDR; National Research Council 2004), instead computing a High Resolution Precipitation Product (HRPP; Turk et al. 2008).

The requirements for the multi-satellite product are summarized in Table 2. The space-time resolution is roughly the microwave spatial scale and the IR temporal scale. The space-time domain represents the PMM goal of covering the whole globe starting with TRMM. Multiple output products are created to satisfy different classes of users, summarized in Sec. 3.2. The term "snapshot" for half-hourly estimates reflects the fact that individual satellite overpasses are the basis for these data, and that the resulting satellite estimates are not "instantaneous", but represent an interval that can exceed an hour (Villarini et al. 2008, O et al. 2017). The best TRMM, and then GPM estimate of precipitation should be taken as the calibration standard. Currently, this is considered to be the GPM Combined Radar-Radiometer (CORRA-G, using GMI and DPR), and an equivalent computation using TMI and PR during the TRMM era (CORRA-T), collectively referred to as CORRA. As well, gauge data are clearly important for anchoring the satellite estimates. Error estimates and auxiliary data fields included in the output files are key to giving users (and developers) the information needed to assess quality by time and region over the life of

the dataset. Finally, as a quasi-operational system, the code must "take a licking and keep on ticking."

3.1 Algorithm Overview

A great deal of expertise in merged precipitation algorithms was developed in the United States during the TRMM era, funded mainly by PMM and by NEWS, NOAA programs (CPO, USWRP), NSF SAHRA, and UNESCO G-WADI (see Sec. 8 for a complete acronym list). IMERG drew on the strengths of the various groups on the PMM Science Team to create a unified U.S. algorithm. Specifics are:

- Perform careful intercalibration of microwave estimates
  - the GSFC group had a strong background
- Provide finer time and space scales to provide users with adequate sampling
  - the CPC group had strong experience with quasi-Lagrangian time interpolation "morphing" using Kalman filters
  - the GSFC group built on this record to refine the process
- Provide microwave-calibrated IR estimates to complement the PMW constellation
  - the CPC group operationally produced (and still produces) the 4-km Merged IR Tb products
  - the U.C.-Irvine group had strong experience in computing IR precipitation estimates
- Incorporate gauge data to control bias
  - the GSFC group had a strong background in monthly corrections
- Provide error estimates
  - both the GSFC and CPC groups brought strengths, although estimates for the native half-hourly 0.1° resolution remain a topic of research
- Deliver and support a code package that runs in the PMM Precipitation Processing System (PPS) environment
  - the GSFC group had a strong track record

The high-level block diagram that results from this analysis is shown in Figure 2, which identifies the institutions that provide the heritage code for the various blocks. Note that this diagram reflects substantial advancements that have been introduced in subsequent versions of IMERG, as summarized in the following descriptions.

Table 2. Notional requirements for IMERG. CORRA refers to the Combined Radar Radiometer Analysis for both the TRMM and GPM eras.

Resolution	0.1° [i.e., roughly the resolution of microwave estimates]
Time interval	30 min. [i.e., the geo-satellite interval]
Spatial domain	global
Time domain	1998-present; later explore entire SSMI era (1987-present)
Product sequence	"Early" sat. (~4 hr), "Late" sat. (~14 hr), "Final" sat.-gauge (~3.5 months after month) [more data in longer-latency products]
Snapshot vs. accumulated	Snapshot for half-hour, accumulation for monthly; data centers provide value-added products for other accumulation periods
Sensor precipitation products intercalibrated to CORRA	

Global, undercatch-adjusted monthly gauge analyses including retrospective product; explore use in submonthly-to-daily and near-real-time products
Error estimates, including "quality"; final form still open for definition
Embedded data fields showing how the estimates were computed
Precipitation phase estimates; probability of liquid phase
Operationally feasible, robust to data drop-outs and (constantly) changing constellation
Output in HDF5 (compatible with NetCDF4); data centers provide value-added products for other formats, and spatial and parameter subsetting
Archiving and retrospective processing for all RT and post-RT products

3.2 Processing Outline

Initial Processing (Sec. 3.2.1) occurs when the IMERG algorithm is run with newly arriving input data, while Retrospective Processing (Sec. 3.2.2), also known as reprocessing, occurs when the IMERG algorithm is run using previously archived input data.

3.2.1 Initial Processing

The block diagram for IMERG is shown in Figure 2. In words, the input precipitation estimates computed from the various satellite PMW sensors are assembled, mostly received at PPS as Level 1 brightness temperatures from the relevant providers, converted to GPM Level 1C intercalibrated brightness temperatures, then converted to Level 2 precipitation estimates using GPROF2021 (currently). All estimates are gridded, intercalibrated to the CORRA product on a rolling 45-day basis using probability matching, and climatologically calibrated to the GPCP monthly estimates with a simple ratio in high-latitude oceans (where CORRA V07 is deficient in precipitation). These microwave data are combined into half-hourly fields and provided to both the Kalman Filter (KF; following Joyce et al. 2011) quasi-Lagrangian time interpolation scheme and the Precipitation Estimation from Remotely Sensed Information using Artificial Neural Networks – Dynamic Infrared-Rain Rate (PDIR; Nyugen et al. 2020a,b) re-calibration scheme. In parallel, CPC assembles the zenith-angle-corrected, intercalibrated merged geo-IR fields and forwards them to PPS for use in the PDIR computation routines. In previous versions of IMERG, the "displacement vectors" needed in the KF quasi-Lagrangian time interpolation scheme were computed from "even-odd" files of the IR data, also supplied by CPC. However, these vectors are now computed from Modern-Era Retrospective Analysis for Research and Applications, Version 2 (MERRA-2) and Goddard Earth Observing System model (GEOS) Forward Processing (FP) data (Sec. 3.3.3), which PPS routinely ingests. The PDIR estimates are computed (supported by an asynchronous re-calibration cycle) and sent to the KF quasi-Lagrangian time interpolation scheme. The KF quasi-Lagrangian time interpolation (supported by an asynchronous updating cycle for the KF weights) uses the PMW and IR estimates to create half-hourly estimates. Note that various intermediate fields are carried through the processing as necessary to populate the fields in the output file (Table 5).

Precipitation phase is computed in the microwave-merger step as a diagnostic using surface type, surface pressure, surface temperature, and surface humidity (Sec. 3.10).

The system is run twice in near real-time:

- "Early" Run ~4 hours after observation time and
- "Late" Run ~14 hours after observation time,

and once after the monthly gauge analysis is received

- "Final" Run ~3.5 months after the observation month.

The baseline is for the Early and Late half-hour land estimates to be calibrated to the Final Run with climatological coefficients that vary by month and location, while in the Final Run the half-hour multi-satellite estimates are adjusted so that they sum to the monthly satellite-gauge combination computed in IMERG (following the TMPA approach). In V06 we chose not to apply climatological coefficients to the Early and Late estimates, believing that there was minimal impact, but in V07 we include it. In all cases, the output contains multiple fields that provide information on the input data, selected intermediate fields, and estimation quality.

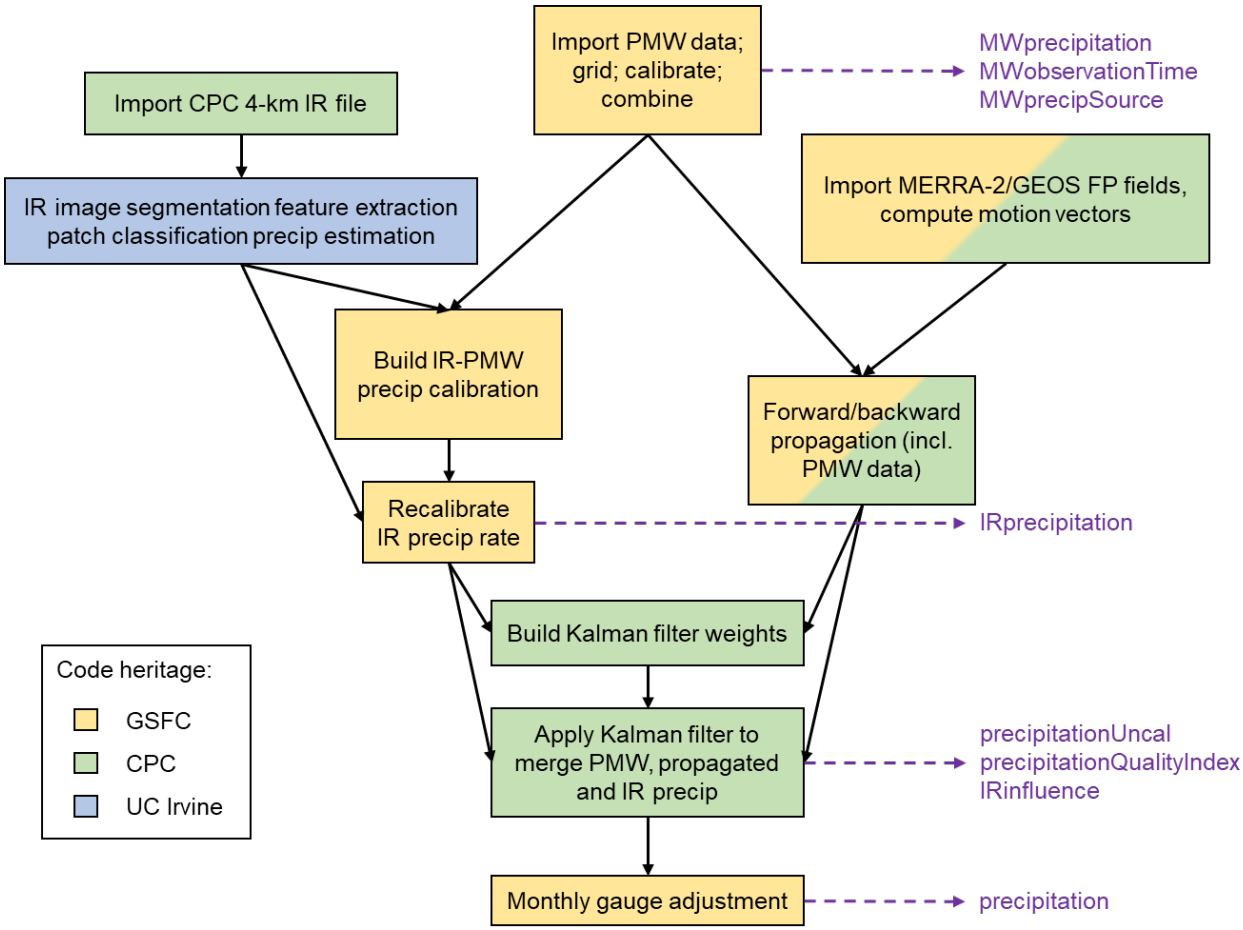

Figure 2. High-level block diagram illustrating the major processing modules and data flows in IMERG, as well as variables that are output to file. The blocks indicate institutional heritage, but the final code package is an integrated system.

Given the multiplicity of Runs discussed here and below, it is key to IMERG maintainability and consistency that all of the Runs share a common code. The different Runs are achieved with options programmed into the single system, even though PPS chooses to install separate instantiations of the code for each Run. The Early and Late Runs are executed in the PPS Real Time (RT) processing system, which focuses on current data, while the Final Run is executed in

the PPS Production processing system. Table 3 summarizes the key differences between the three Runs.

Table 3. Summary of the key input and algorithmic differences between the Early, Late, and Final Runs.

Run (latency)	Early (4 hours)	Late (12 hours)	Final (3.5 months)
GPROF product	Near-real-time	Near-real-time	Climate
Fraction of input PMW sensors	95%	100%	100%
CORRA product	Near-real-time	Research	Research
CORRA calibration	Trailing 45-day	Trailing 45-day	Centered 45-day
Motion vector source	GEOS FP	GEOS FP	MERRA-2
PMW propagation	Forward only	Forward and backward	Forward and backward
Kalman correlation window	Trailing 3-month	Trailing 3-month	3-month with one-month off-center
Gauge adjustment	Final Climatological	Final Climatological	GPCC analysis
PLP source	JMA Forecast	JMA Forecast	ERA5
Others	No manual inspection	No manual inspection	Visual inspection for bad PMW and IR, manually flagged for removal

3.2.2 Retrospective Processing

Retrospective processing, also known as reprocessing, is key to creating a consistent dataset. This consideration is relevant to users of all three Runs of IMERG, so all three Runs are reprocessed. By design, the Production processing system, which computes the Final Run, supports reprocessing. The RT processing system, which computes the Early and Late Runs, does not support reprocessing. This issue is addressed by retrospectively processing IMERG in the Production system with calls that mimic the processing for Early and Late. Because the time of arrival of the input files is not tracked, the selection of input data available to the retrospective Early and Late Runs is a superset of the input data covering the original Early and Late, and the input data from a particular sensor are produced by the "climo" GPROF estimates (computed with more-carefully prepared reanalysis data). In a future release, we may decide to institute climatological calibrations in the retrospective Early Run that are different from those in the Early. The same approach is possible for the Late.

When a new version of IMERG is released, retrospective processing the Early and Late Runs is carried out after reprocessing the Final Run to allow computation of climatological coefficients that calibrate Early and Late to the Final monthly product (which has gauge information). Note that in V06 we could not do this last calibration, but it is included in V07. This approach allows use of intermediate Final results already computed, shortening the processing cycle. This comes at the expense of using a superset of the data that actually were available in real time (i.e., also using data that came in after what would have been received in time for the original near -real-time computation), and perhaps some slightly different calibrations.

3.2.3 Rotating Calibration Files and Spin-Up Requirements

There are three calibrations that require routine rotating accumulators in IMERG. First, there is the primary calibration of precipitation products, which in the TRMM era is carried out as TMI calibrated to CORRA-T, and in the GPM era is carried out as GMI calibrated to CORRA-G. This calibration is done over an interval of nine 5-day periods (nine pentads) for stability. [Recall that the TMI and GMI products are used as calibrators for all the other satellite precipitation estimates. This is done because direct matchups between CORRA-T or CORRA-G with the other sensors are exceedingly sparse.] TMI is reduced to the status of being just another high-quality sensor during the period in which GMI is acting as the calibrator, and vice-versa. The rotating calibrations are necessarily trailing in the Early and Late Runs, but we use an approximately centered approach for the Final Run.

The second rotating accumulator is for the Kalman filter, whose statistics are currently calibrated over a 3-month period. A side study showed that this interval yields results very similar to a 5-month period. Here too, the Early and Late Runs use trailing calibrations, while the Final Run is approximately centered in time.

The third rotating accumulator is for the PMW calibration of PDIR, which uses an interval of six pentads (30 days) for stability. This accumulator file is trailing for the Early and Late runs and centered for the Final run.

There are also a number of calibrations that are currently climatological, but have the potential to be converted to rotating calibration files in the future if further research shows that the climatological approach is insufficiently accurate. These include the various calibrations of other sensor precipitation datasets to TMI and GMI in their respective eras.

The final issue for the rotating accumulation files is providing seed and restart files. When the data are eventually processed back to January 1998, the development team will provide the start-of-record seed files for TRMM. Thereafter, in normal operations the rotating files are programmed to refresh as new data arrive. In the interim, while IR data are only available starting in February 2000, the start-up is provided by accumulating calibration data for the first several months of input data and then releasing data starting with June 2000. This ensures that the subsequent calibrations for earlier data will mesh smoothly with the calibrations applied in the previously released data. The start-up for the GPM era is provided by similarly accumulating calibration data for the first 3 months of Core Observatory data and then switching from TRMM-based to GPM-based calibrations starting with June 2014. Occasionally throughout the mission, it is likely that processing difficulties, bad input data, or undetected code errors will force a restart of processing. To accommodate such cases, PPS saves daily dumps of rotating accumulation files and all the intermediate files.

3.3 Input Data

3.3.1 Sensor Products

The sensor products are detailed in Sec. 2 as part of the discussion of the various sensors. For the most part, the datasets listed in Table 1 from previous and current sensors have already been archived at PPS under TRMM, and then GPM operations, but the requirement is that all inputs be processed using the current GPM version of GPROF2021. As such, we work closely with the GPROF developers at Colorado State Univ. and with PPS in testing to ensure the best quality products.

Note that the V07 GPROF estimates for AMSU-B, ATMS, and MHS do not provide estimates for the 5, 8, and 5 footprints (respectively) at each swath edge. This is due to algorithm issues as revealed in IMERG V06 testing. Taken together, these limitations somewhat reduce the amount of microwave-based data contained in Version 07 IMERG. Future reprocessings might address these issues.

3.3.2 Ancillary Products

The ancillary products required on a routine basis for the IMERG algorithm are surface type, surface pressure, surface temperature, and surface relative humidity. Surface type is provided by the standard static map of percent water coverage from PPS. Surface pressure, surface temperature, and surface relative humidity are provided by the JMA forecasts for Early and Late Runs of meteorological data. The Final Run uses the ECMWF Reanalysis version 5 (ERA5) product for consistency with the "climatological" run of GPROF2021.

3.3.3 MERRA-2 and GEOS FP Products

MERRA-2 is a global atmospheric reanalysis beginning in 1980 using the Goddard Earth Observing System Model, Version 5 (GEOS-5) data assimilation system and numerical model (Bosilovich et al. 2016; Gelaro et al 2017). GEOS Forward Processing (FP) is a global forecast analysis using the GEOS-5 system run every 6 hr (Lucchesi 2018). Both datasets are processed and released by the NASA Global Modeling and Assimilation Office.

The precipitation (PRECTOT), total precipitable liquid water (TQL), and total precipitable water vapor (TQV; also called total column water vapor) are used in V07 to compute the motion vectors for propagating the PMW data. PPS extracts all data fields from daily files of hourly data at 0.5° × 0.625° latitude/longitude for MERRA-2, and from hourly files at 0.25° × 0.3125° latitude/longitude for GEOS FP, feeding into post-real-time and retrospective processing, and near-real-time processing, respectively.

GEOS FP is episodically upgraded as research progresses. The IMERG team considers the impact of each such upgrade, but in general they are minor compared to the approximations involved in computing the displacement vectors.

3.3.4 GPCP SG Product

The GPCP is an international, community-based activity of the Global Energy and Water Exchange (GEWEX) project that produces long-term, global, climate-oriented precipitation datasets. The Satellite-Gauge (SG) product is a monthly analysis on a 0.5°x0.5° grid for 1983 to the near-present. It merges various satellite-based estimates over both ocean and land, combined with the precipitation gauge analyses over land from the GPCC. The satellite-based estimates are IR-based, calibrated by passive microwave estimates for the latitude band 35°N-S, rolling over from passive microwave calibrated IR to microwave sounders in the latitude range 35°–58°NS, and adjusted microwave sounders in the latitude range 58°–90°NS. The algorithm, currently at V3.2, is described in Huffman et al. (2023) and prior papers referenced therein. A significant effort is made in GPCP to enforce homogeneity on the input data sets and the resulting merged analysis across the span of the analysis to meet CDR standards. Where possible, this includes using an overlap time period to adjust for data and/or algorithm differences and to remove data source artifacts.

3.3.5 NOAA Autosnow Product

The NOAA Autosnow product is used to provide global data on daily surface coverage by snow and ice. Currently, information on the snow cover is derived from the Advanced Very High Resolution Radiometer (AVHRR) onboard METOP satellites, imagers onboard Geostationary Operational Environmental Satellites (GOES) East and West, Spinning Enhanced Visible and Infrared Imager (SEVIRI) onboard Meteosat second Generation (MSG), and Special Sensor Microwave Imager/Sounder (SSMIS) onboard Defense Meteorological Satellite Program (DMSP) satellites. Ice cover is derived from the METOP AVHRR and DMSP SSMIS data. Both snow and ice are identified in satellite images using threshold-based decision tree image classification algorithms. Information on snow and ice cover derived from observations in the visible/infrared and the microwave bands is combined to generate continuous (gap-free) maps on a daily basis. The main output product of the system is a daily global snow and ice cover map generated on a 0.04° lat/lon grid (Plate Carree), which is about 4×4 km at the Equator. On July 1, 2023, the Autosnow product transitioned to the 0.02° lat/lon grid resolution. See Romanov (2016) for more details. This version ended use of SSMIS.

The Autosnow product is used in the Kalman filter to reduce the Quality Index of PMW and propagated retrievals over frozen surfaces.

In V07, IMERG uses all microwave estimates in the merge and propagation steps, providing global coverage, albeit with lower Quality Index over frozen surface.

As of 14 June 2019, it was discovered that Autosnow sometimes provides incorrect values other than "sea ice" above 89°N. At the time, these values caused IMERG to treat these boxes as other than sea ice. This error was corrected in V07.

3.4 Microwave Intercalibration

The IMERG precipitation estimates are calibrated to the TRMM/GPM single- or combined-sensor estimates deemed highest-quality following Huffman et al. (2007), currently the CORRA estimates. During the initial release period in the GPM mission a short-record (6-9 month-based) calibrator was used, pending a longer GPM-based calibrator, while in V05 and V06 it was seasonal averages for 2015. The microwave intercalibration technique is based on quantile-quantile matching, similar to Miller (1972) and Krajewski and Smith (1991). The temporal and spatial scale of the histogram matching for any given sensor depends upon the unique orbit and individual sensor characteristics. Vastly different orbits, leading to fewer data overlaps, may require a longer calibration period to ensure representative geographic and diurnal sampling. Similarly, radically different sensors may require sampling at higher spatial and temporal resolution. Climatological (fixed, generally seasonally varying) calibrations are used when possible, with dynamically-computed (monthly, say) calibrations utilized when necessary.

The CORRA-T and CORRA-G calibrations are computed on a 1°x1° grid using a 3°x3° template. Experience in V03 showed that regions with differing gradients in GMI and CORRA resulted in blocky patterns when the calibrations were used on the original 1° grid. So, starting in V05, the calibrations used were distance-weighted interpolations of the four surrounding 1° calibration values.

For V07 the IMERG team worked with the PPS and GPROF teams to determine that the original GMI/TMI precipitation rate histograms within the radar swath exhibited small but systematic differences from the histograms computed for just the parts of the GMI/TMI swath outside the radar swath. In Figure 3 and Figure 4 we evaluate along-scan beam position precipitation biases

in the V07 GPROF-GMI/TMI retrievals and show examples of the associated biases when calibration is computed with coincident GMI/TMI and 2BCMB data, then applied to the full GMI/TMI swaths. To resolve these biases, we compute the calibrations using the full GMI/TMI swath and the narrower 2BCMB retrievals. Despite the lack of complete spatial coincidence in this approach, we demonstrated the improvement of the 2BCMB-GMI/TMI calibration. Given the central role of PMW retrievals in IMERG, these improvements lead to increased accuracy in the IMERG product. Figure 3 demonstrates the ability of close CORRA-T calibrations of TMI using calibrations from only temporally and spatially coincident CORRA-T and TMI in spatial and temporal collocated retrievals [top panels], however generally the calibrations are too high when comparing the full swath of calibrated TMI with CORRA-T [bottom panels]. Figure 4 demonstrates CORRA-T calibrations of TMI using calibrations derived with only temporally coincident but full swath TMI reveal close zonal profiles of calibrated TMI and CORRA-T in temporal collocated retrievals [top panels], however also the calibrations are close when comparing the full swath of all calibrated TMI with CORRA-T [bottom panels].

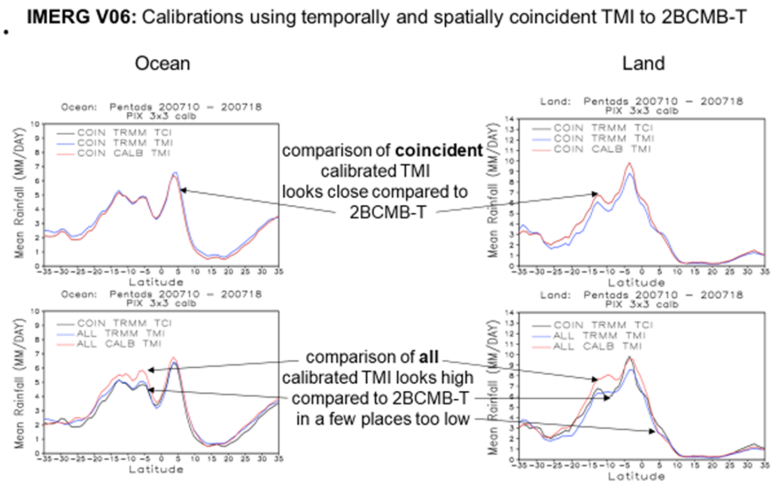

Figure 3. CORRA-T calibrations of TMI using calibration from only temporally and spatially coincident CORRA-T and TMI reveal close zonal profiles of calibrated TMI and CORRA-T in spatial and temporal collocated retrievals [top panels], however generally the calibrations are too high when comparing the full swath of calibrated TMI with CORRA-T [bottom panels].

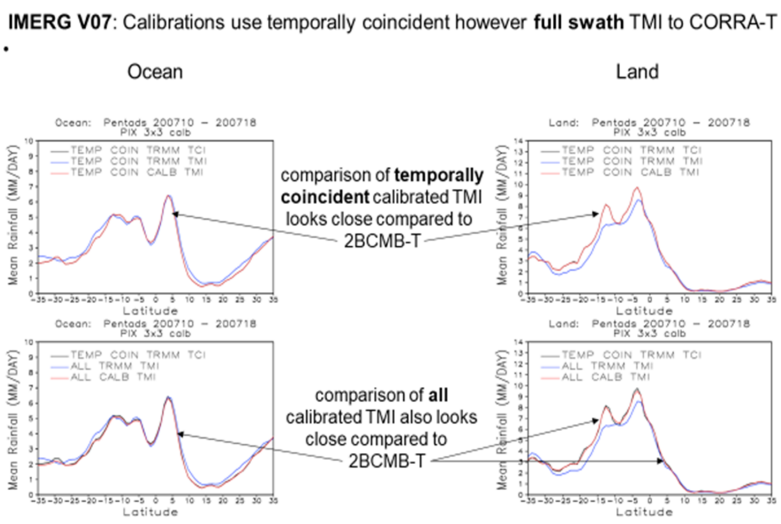

Figure 4. CORRA-T calibrations of TMI using calibrations derived with only temporally coincident but full swath TMI reveal close zonal profiles of calibrated TMI and CORRA-T in temporal collocated retrievals [top panels], and also the calibrations close comparing all periods of full swath of calibrated TMI with CORRA-T [bottom panels].

The TMI- and GMI-other-satellite calibrations are computed on 22 15° zonal histogram bands overlapping at 5° increments for ocean. A single histogram is used for land due to sampling concerns. Experience in V03 showed that zonal bands with differing gradients between GMI and cross-track sounders occasionally resulted in zonal discontinuities when the calibrations were used on the center 15° band. So, the sounder calibrations are equal-weighted averages of the upper, center, and lower band calibration values. However, testing for V05 showed that high-rate grid boxes were badly overestimated in this process, so GMI-other-satellite calibrations were not carried out in V05 except for SSMIS, whose PDF of GPROF precipitation rates differed from the other constellation sensors. In V06 and subsequently V07, all constellation satellites are intercalibrated to TMI and GMI using the ocean and land histogram technique previously described. The cross-track scanners employ the equal-weighted average of the upper, center, and lower ocean band values but the conical scanners do not. The results showed that constellation satellite calibration to GMI was challenging due to the sampling as a result of the GPM orbit and the sun-synchronous satellite orbits. SSMIS was significantly overcorrected over land so it was decided to leave the SSMIS estimates as is. Due to sparse sampling, TMI was not calibrated to GMI and is used as is. Calibration of constellation satellites to TMI in the TRMM era proved more stable and all satellites are intercalibrated.

KF, PDIR, Early, and Late all use various lengths of trailing calibration in which updating is considered necessary, and this is the intended approach for the near-real-time IMERG Runs. The post-real-time TMPA used a calendar-month calibration, but for consistency across the IMERG Runs, we routinely update the Final calibrations such that each day is approximately in the middle of the calibration period except for the Kalman statistics computation which is uses the current and two previous months so it is at the end of the calibration period.

One improvement in GPM over TRMM is that both DPR and CORRA-G are available in real time, whereas PR and TCI were not in TRMM. This allows us to have the same calibrating sensor for all the IMERG runs in Initial Processing (i.e., computations with newly received data).

Even though CORRA is considered to be the best estimator, in V07 (as in V04, V05, and V06) all of the GPM individual-sensor precipitation products are biased low in the high latitude oceans compared to the GPCP Satellite-Gauge product and estimates based on CloudSat (Behrangi et al. 2014 and subsequent revisions to the approach). There is some variation between the latter two, but the GPCP can provide regionally varying monthly climatological adjustment factors, while the CloudSat-based data currently only have an annual latitudinal profile over ocean. Thus, in V07 (as in V04, V05, and V06) we are making a simple ratio adjustment over ocean to bring the CORRA-calibrated constellation estimates in line with what is considered a more reasonable estimate. We apply these corrections outside of a somewhat subjectively chosen, seasonally varying low-latitude zone (around 30°N-S) where the ratio of CORRA to GPCP is close to one. Finally, in the TRMM era the CORRA-T calibration must be extended out from 35°N and S to higher latitudes. In TMPA this was done with a smooth-fill*, which proved to yield problematic results in the cold season, but now the extension can use the actual CORRA-G values to more closely approximate the extension. Calibration outside the CORRA-T area of coverage in the GPM era is provided by extrapolating the northernmost and southernmost CORRA-G correction curves at 60º N and S to the poles using a 50-pass iterative smooth-fill technique to obtained corrections in the latitude bands 60º-90º N and S. To add stability to the extrapolated correction curves, the zonal mean of the corrections is computed at 60º N and S and assigned to the 90º N and S zonal bands, respectively.

In the TRMM era, background monthly climatological GPM-era GMI-CORRA histograms and correction curves are used to fill in the corrections for the latitude bands 33º-90º N and S. This fill in is performed as follows:

1. Compute the count-normalized precipitation volumes for CORRA-G and CORRA-T in the latitude bands 0º-33º N and S using the TMI-CORRA month and GMI-CORRA background histograms.
2. Compute volume adjustment factors for northern and southern hemisphere ocean and land.
3. Apply these volume adjustment factors to the GPM background correction curves.
4. Insert the volume-adjusted GPM correction curves into the T-CORRA correction curves in the region 25º-90º N and S, performing a weighted average of the two corrections in the latitude bands 25º-33º N and S.

The resulting corrections are based on TRMM for the latitude band 25ºN-25ºS, volume-adjusted GPM for the latitude bands 33º-90º N and S, and a blend of the two in the latitude bands 25º-33º

* The smooth-fill algorithm provides smoothly varying values for one or more grid boxes with "missing" values that match the non-missing boxes around the edge of the "missing" hole. At each step of the iterative process, each originally missing boxes is filled with the 3x3-gridbox average of the non-missing box values in the previous iteration. Preliminary analysis showed that the innovations in the missing grid boxes substantially settle down when the number of iterations is 6 times the number of iterations it takes to give each missing grid boxes a value. For the CED grid, all grid boxes at the pole are given the same value.

N and S. The goal is to provide the GPM correction structure outside the TRMM coverage area, but with the volume of the TRMM estimates. This was necessary, as directly extrapolating the TRMM region corrections to the poles created artificially low corrections.

3.5 Merged Microwave

The intercalibrated microwave precipitation estimates from GMI, TMI, and all of the partner sensors in the constellation are merged to create Level 3 data sets containing the best observational data available in each half hour. All of the input data sets are gridded from their native Level 2 swath data to the IMERG 0.1°x0.1° Level 3 global grid on the IMERG half-hourly interval (namely the first and second half hour for each UTC hour). The grid is populated with sensor data in the priority order conical-scan radiometer, and then cross-track scanner. [Note: this is a good choice over ocean, but not necessarily for land areas.] If there is more than one sensor in a class, the one closer to the center of the half hour is chosen. The precipitation estimate, sensor type, and time of observation (to the nearest minute) are reported in the output data set.

3.6 Microwave-Calibrated IR

Geo-satellites give frequent sampling, but the resulting IR Tb data are related to cloud top features (temperature and albedo) rather than directly to surface precipitation. This indirect relationship is best captured if the IR Tb-precipitation relationship is improved using texture and patch classification as well as applying routine updates using leo-PMW based precipitation estimates. Here, following the PDIR (Nguyen et al. 2020a,b) is based on the framework of the PERSIANN-Cloud Classification System (PERSIANN-CCS, Hong et al. 2004), which is in turn based on the original PERSIANN framework (Hsu et al. 1997, Sorooshian et al. 2000). PERSIANN and PERSIANN-CCS, along with PERSIANN-Climate Data Record (PERSIANN-CDR, Ashouri et al. 2015), are satellite-based data-driven precipitation estimating systems that use machine-learning techniques to establish a link between GEO cloud-top brightness temperature (Tb) and RR. PDIR advances the framework of the PERSIANN-CCS system by (i) improving the capture of warm precipitation by including a higher temperature threshold; (ii) introducing gradient filtering and applying morphological filters to improve the watershed method used for segmentation; (iii) expanding the cloud classification system to include monthly sets of cloud types, thus improving the algorithm's ability to distinguish between different rainfall regimes; (iv) improving the skill of the Tb–RR curves with IMERG Merged PMW precipitation dataset; and (v) utilizing gridded climatology data from WorldClim version 2 (Fick & Hijmans 2017), and PERSIANN-CDR to create a dynamical Tb–RR curve model, optimized by the shuffled complex evolution optimization algorithm (SCE-UA; Duan et al. 1994). The central hypothesis behind PDIR is that characteristics related to the land surface below the clouds (topography, elevation, climate type, temperature climatology, etc.) play a role in the cloud-top temperature–rain rate (Tb–RR) relationship of clouds. In order to create a dynamic relationship between input IR-measured Tb and output RR, rainfall climatology values influenced by the unique land surface characteristics inherent to a region, are used to "slide" the Tb–RR curve along the Tb axis. This results in identical clouds with identical Tb intensities and distributions having different pixel RR values when occupying spaces with differing rainfall climatology.

3.7 Kalman Filter Time Interpolation

Under the Kalman filter framework as originally developed in CMORPH and extensively modified for use in IMERG, the precipitation analysis for a grid box is defined in three steps (Joyce et al.

2011). First, the half-hourly PMW estimates of snapshot precipitation rates closest to the target analysis time in both the forward and backward directions are propagated from their observation times to the analysis time using the motion vectors computed from the selected numerical model and reanalysis fields (see next paragraph). The "prediction" of the precipitation analysis is then defined by compositing the forward- and backward-propagated PMW estimates with weights proportional to the square of their correlation against GMI/TMI. In contrast to previous IMERG versions in which snapshot PMW observations are excluded from the Kalman filter list and passed straight through to the final satellite-only estimate, in V07 the propagated precipitation includes snapshot PMW estimates where present. The exception to this rule is propagated sounder observation when snapshot imager data are also available over ocean, in which case the propagated sounder is not considered in the Kalman filter due to its notably lower performance (You et al. 2021). If the time interval from the nearest PMW observation is longer than 30 minutes, the final "analysis" is defined by updating the "forecast" with IR-based precipitation observations. The weights used in the Kalman filter are proportional to the square of the observational correlations. This 30-minute threshold is due both to the natural timescale of precipitation at these fine scales and to the retrieval errors in the microwave algorithms.

Up through V05, the motion vectors used to propagate the PMW estimates were calculated by computing the pattern correlation between spatially lagged geo-IR Tb arrays from two consecutive images, effectively reflecting the large-scale motions of cloud tops as in the original CMORPH. In V06, the source of the motion vectors was switched to total precipitable water vapor (TQV) from the MERRA-2 (for the Final Run) or from GEOS FP (for the Early and Late Runs), which was demonstrated to better capture the motions of precipitation systems while providing full global coverage (Tan et al. 2019). In V07, following studies revealing deficiencies in these TQV motion vectors near orography (e.g., Derin et al. 2019), the motion vector source is modified from the single TQV variable to a hierarchy of three variables: precipitation (PRECTOT), total precipitable liquid water (TQL), and TQV. Specifically, motion vectors are first computed from PRECTOT where available; if unsuccessful due to the absence of model precipitation, the motion vectors are then computed from TQL; and if that is unsuccessful because the TQL field is too dry, the scheme will fall back to the (globally complete) TQV. Occasionally, PRECTOT and TQL vectors in a location are appreciably different from their surrounding values, especially when the magnitude of the fields is small, in which case they are removed and populated by vectors from the successive field. It should be stressed that model precipitation (and other fields) are used only to determine the large-scale motions and none of the model field values (precipitation in particular) are incorporated into the final IMERG precipitation rates, so issues arising from model limitations in estimation of precipitation rates are not a concern here. Stated differently, it is the patterns of PRECTOT, TQL, and TQV that matter, not their dimensional values.

Following the KF approach used for the geo-IR Tb fields, the motion vectors are computed by identifying the spatial offset between two consecutive hourly fields of the local "scene" that give the highest correlation. This scene is defined as a box with a latitude length of 5° and a longitude length that is equivalent to 5° at the equator (and increases in the longitudinal size measured in degrees at higher latitudes to approximately preserve the same physical distance). Motion vectors are computed at every 2.5° × 2.5° globally, then downscaled by bilinear interpolation to the 0.1° grid. The hourly resolution of MERRA-2 and GEOS FP means that the computed motion vectors have to be linearly interpolated to the half-hourly timescale. The end result is a global field of motion vectors at 0.1° every half-hour that can be used to propagate the PMW precipitation in time. In V06 and earlier versions, the same set of vectors are used to propagate the PMW

precipitation both forward in time as well as backward in time by "flipping" the vectors. However, it was realized that "flipping" the vectors for backward propagation can introduce a slight positional error. [Effectively, "flipping" the vectors meant that the positions of the head and the tail of the arrow are switched, which introduces a spatial offset if not accounted for.] Hence, motion vectors in V07 are computed separately for forward propagation and backward propagation. The units are in whole grid boxes in the longitudinal and latitudinal directions, so the half-hour displacements are somewhat approximate.

In V07 four precipitation fields feed into the Kalman filter: the snapshot PMW precipitation field, the forward propagated PMW precipitation field, the backward propagated PMW precipitation field, and the IR precipitation field. In V06, snapshot PMW estimates were not ingested into the Kalman filter and were instead passed straight to the satellite-only field on the assumption that the Kalman filter should only fill in the gaps in the high quality PMW field). However, propagated precipitation may carry useful information in addition to the snapshot PMW estimates, which led to including the snapshot PMW estimates in the Kalman filter for V07. This effectively combines the snapshot PMW retrievals with propagated precipitation, and thus elevates the Kalman filter from a gap-filling tool to a method to combine multiple sources of information. A specific exception is implemented to exclude propagated sounder estimates in the presence of snapshot imager estimates over ocean based on tests showing lower information content in sounder channels for oceanic precipitation retrievals (You et al. 2021). Overall, this leads to reduced inter-sensor differences and slightly improved performance. [If a user prefers the V06 approach of using the PMW estimates unchanged, they could insert the non-missing values from the *MWprecipitation* variable into the *precipitation* data field.] The four fields are averaged at each 0.1° grid box with weights inversely proportional to their KF errors. Expressed in the form of correlation, these seasonally and regionally dependent errors are calculated by comparing the sensor type (imager, sounder, or IR) against collocated TMI/GMI observations. Specifically, the correlations are derived over a three-month period, off-centered on the nominal month for the Final Run (e.g., for May, the correlations are computed over March-April-May) and trailing the nominal month for the Early and Late Runs (e.g., for May, the correlations are computed over February-March-April). [Ideally, the three-month window for the Final Run should be centered on the nominal month, but a one-month shift was introduced to facilitate initial processing since tests indicated that the differences are negligible.] Over land, the correlations are computed at each 10° band using data over a 30°-wide latitude band centered on the target band. Over ocean, the correlations are computed for each 20° × 20° box using data over a 60° × 60° region centered on the target box. Both the 3-month window and the large regions are selected to ensure robust statistics, with additional post-processing to ensure reasonable behavior (e.g., by capping the correlation of propagated precipitation at +2.5 h to be no greater than the correlations of propagated precipitation at +2.0 h). Due to the manner in which the PMW field is handled in the current implementation of IMERG, it is not possible to calculate the "t = 0 h" correlations between the snapshot PMW estimates and GMI/TMI in the Kalman filter. Lacking strong justification for alternatives, they are approximated by first computing a set of monthly baseline correlations from gridded and intercalibrated GPROF estimates from December 2014 to November 2015, then included into the Kalman correlations with dynamical adjustments based on the adjacent "t = ±0.5 h" correlations (i.e., correlations against GMI/TMI of the PMW estimates propagated forward and backward in time by one half-hour). With these correlations, the Kalman filter averages the input estimates at each 0.1° with weights proportional to the square of the (positive) correlation.

Up through V06, concerns over the performance of PMW retrievals over frozen surfaces had led to a policy of screening these estimates over frozen surfaces as flagged by the NOAA Autosnow product. This meant that estimates over frozen surfaces comprised solely of IR precipitation within 60°N/S and were masked at higher latitudes beyond IR coverage. With evidence emerging to the contrary (e.g., Arabzadeh and Behrangi 2021), for V07 an investigation into this issue confirmed that GPROF 2021 PMW retrievals, while having diminished performance, still carry useful information and generally outperform IR retrievals (personal communication with P. Kirstetter 2023). Therefore, the longstanding policy of screening out PMW retrievals over frozen surfaces is lifted in V07. The result is that, except for a handful of grid boxes mostly at the poles, IMERG has complete global coverage, with snapshot and propagated PMW estimates covering the polar regions. Nevertheless, users should be aware of the diminished performance of these estimates and exercise appropriate caution when interpreting the results. In particular, applications that use and evaluate these estimates over frozen surfaces, especially at high latitudes, should indicate this caveat of reduced skill in the interpretation of their results. This reduced skill is flagged by decreasing the Quality Index (see Sec. 3.12.1).

A major issue identified in a study using V06 data is the fact that the averaging of multiple precipitation fields in an Eulerian framework can lead to a distorted distribution in the precipitation rates, such as an inflated precipitation area and suppressed intense occurrence (Rajagopal et al. 2021). In response, the Scheme for the Histogram Adjustment of Ranked Precipitation Estimates in the Neighborhood (SHARPEN) was developed to mitigate this issue (Tan et al. 2021) and implemented in V07. Inspired by quantile mapping, the scheme compares each averaged value from the Kalman filter to the surrounding KF estimates, calculates its rank among its neighbors, and replaces this averaged value with the value of the same rank from the input fields over the same region weighted by Kalman weights. Taking a simplified example, if a value from the KF is at the 75th percentile compared to its neighboring KF estimates (all of which have experienced some level of averaging), SHARPEN will replace it with the 75th percentile value from the weighted histogram of parent fields over the same region. The neighborhood is set at 2.5° × 2.5° centered on the grid box of interest. However, as this process can be resource intensive due to the need to sort two sets of values for each 0.1° grid box, it is expedited by replacing 3 × 3 values for each sorting (see Section 4—or "stride"—in Tan et al. 2021). The output of SHARPEN improves the distribution of the precipitation rates from the Kalman filter, leading to improved representation of precipitation area and intense precipitation occurrence. However, the adoption of SHARPEN complicates the quantification of the contribution of IR precipitation, which was recorded in the variable *IRkalmanFilterWeight* in V06 and prior. What used to simply be a fraction of the weight from IR is muddied by the fact that, even if the nominal grid box has no IR in its Kalman filter input (i.e., *IRkalmanFilterWeight* = 0%), it can still be influenced by the IR field through the 2.5° × 2.5° neighborhood. As such, the *IRkalmanFilterWeight* as previously defined may be misleading. Hence, in V07, *IRkalmanFilterWeight* is replaced by *IRinfluence*, which is computed as the overall fraction of IR weights in the 2.5° × 2.5° neighborhood in SHARPEN. These V07 changes in quantifying the IR contribution and including snapshot PMW estimates in the Kalman filter collectively introduce additional complexity in evaluating contributions by the various input data sources (e.g., Tan et al. 2015, Gebregiorgis et al. 2018). Procedurally, SHARPEN is implemented after the Kalman filter. Note that SHARPEN is not a downscaling scheme, but a scheme that works at the native 0.1° gridbox scale to mitigate the distortion in precipitation rate distribution due to averaging.

3.8 Satellite-Gauge Combination

For the baseline post-real-time IMERG package, we follow the TMPA approach for infusing monthly gauge information into the fine-scale precipitation estimates (Huffman et al. 2007). All of the full-resolution half-hour multi-satellite estimates in a month are summed to create a monthly multi-satellite-only field. This field is combined with the monthly GPCC precipitation gauge analysis (over land) in several steps. First, the gauge analysis is audited to remove isolated island stations, many of which are not representative of the grid box in which they reside. Then the gauge analysis is adjusted for undercatch by multiplying the monthly precipitation values by the corresponding month's gridbox climatological adjustment ratios from Legates and Willmott (1990), with a climatology of the Fuchs et al. (2001) adjustment to reduce the excessive correction north of 45°N over Eurasia. Third, the multi-satellite estimate is adjusted to the large-spatial-scale mean of the gauges, and finally, the adjusted multi-satellite and gauge fields are combined using weighting by inverse estimated error variance. This monthly satellite-gauge combination is a product in its own right (see Table 5). In addition, the field of ratios between the original monthly multi-satellite and monthly satellite-gauge fields is computed, then each field of multi-satellite precipitation estimates in the month is multiplied by the ratio field to create the "calibrated" half-hourly IMERG estimates. In V03 we found that the 1° GPCC data grid caused unphysical blockiness along coasts, so starting in V04 we trimmed the gauge contribution to the coast and dropped isolated islands as not representative of the predominantly oceanic conditions. Furthermore, the GPCC data volume adjustment caused blockiness over land, so it was removed. The net effect is to "spread" the gauge analysis precipitation values for a particular grid box to the surrounding grid boxes. To date, the resulting smoothing has not been considered a significant problem. The satellite-gauge estimates are global, but considered less reliable over frozen surface.

3.9 Post-Processing

IMERG ends with a precipitation post-processing step that introduces gauge information into the original multi-satellite-only half-hourly data (carried as field *precipitationUncal*). For the Final Run, the ratio between the monthly accumulation of half-hourly multi-satellite-only fields and the monthly satellite-gauge field is computed, then each half-hourly field of multi-satellite-only precipitation estimates in the month is multiplied by the ratio field to create the completed half-hourly calibrated IMERG Final Run precipitation estimates in the variable *precipitation*.

The ratio between the monthly satellite-gauge and the monthly accumulation of half-hourly multi-satellite-only fields is limited to the range of 0.2 to 3. The value was moved to 3 from the TRMM V6 value of 2 because testing showed that it did a better job of matching the two accumulations, while a value of 4 started introducing unrealistic shifts to the histogram of half-hourly precipitation rates for the month. Early in TRMM the lower bound was set to 0.5, but it was argued that a smaller value allows matching between the two accumulations without creating the egregious high snapshot values that result when the upper bound is expanded too far.

The baseline IMERG near-real-time products follow the TMPA procedure in providing both the original multi-satellite estimate and a climatologically calibrated field. The climatological calibration is intended to make the near-real-time products as consistent as possible with the Final product. One important simplification compared to the TMPA is that both the DPR and CORRA-G are computed in real time for GPM. This contrasts to the situation in TRMM where the PR and TCI were not computed in real time and we had to substitute TMI as the RT calibrator.

Accordingly, in GPM we compute a straightforward calibration to the Final product using a climatological CORRA-G calibration. If the sub-monthly precipitation gauge combination option is incorporated in the Late product, presumably the need for post-processing will have to be re-assessed, but the Early product is certain to require the climatological calibration to the Final product. Note that this latency is not an issue in computing TMI-CORRA in the TRMM era retrospective processing.

3.10 Precipitation Phase

The precipitation phase, namely whether it is liquid, solid, or mixed, is not currently provided as a satellite-based calculation by the standard PMW precipitation algorithms, so we must use ancillary data sets to create the estimate. Formally, there should be separate estimates for each phase. However, mixed-phase cases tend to be a small fraction of all cases, and we consider the estimation schemes to be sufficiently simplistic that estimating mixed phase as a separate class seems unnecessary. Some users need information on the occurrence of the solid phase, both due to the delays it introduces in moving precipitation water mass through hydrological systems, and due to the hazardous surface conditions that snow and ice create. Accordingly, we lump together liquid and mixed as "liquid" and compute a simple probability of liquid phase. [Note: a value between 0 and 100% gives the estimated probability that the precipitation is liquid; it does *not* denote a mixture in which the fraction gives the precipitation that is liquid and the converse of which is therefore solid. By far, the most likely event is either "all liquid" or "all solid", and the probability of each is the fraction and its converse, respectively. Reports indicate that mixed phase is more common in the Southern Ocean, an issue that is a matter of current research.]]

For the half-hourly data, we adopt the scheme by Sims and Liu (2015), in which the precipitation phase is diagnostically estimated as probabilities using lookup tables—separately over ocean and over land—based on the wet-bulb temperature. These probabilities are derived by comparing station- and ship-based observations of precipitation phase and wet-bulb temperature. In V07, these lookup tables are updated for ERA5 thermodynamic variables (personal communication with G. Liu 2021). Additionally, the probabilities are fitted to logistic functions (or S-shaped curves) to ensure monotonicity and smoothness, so the V07 probability of liquid phase (PLP) is given by,

$$\mathrm{PLP} = \frac{1}{1 + exp\big(-b(T_w - a)\big)},$$

where T_w is the wet-bulb temperature in °C, and a and b are parameters from the fitting performed separately over ocean and land as well as positive and negative values of T_w (Table 4). This V07 PLP functions are shown in Figure 5. For the Final Run, the PLP is estimated from the lookup tables using wet-bulb temperature from ERA5; for the Early and Final Runs, the PLP is estimated using JMA Forecast data.

Table 4: Parameters for the PLP curves.

Surface	T_w sign	a	b
ocean	-	2.3096	0.4881
ocean	+	1.0116	1.1165
land	-	1.9560	0.6898
land	+	0.7349	1.6958

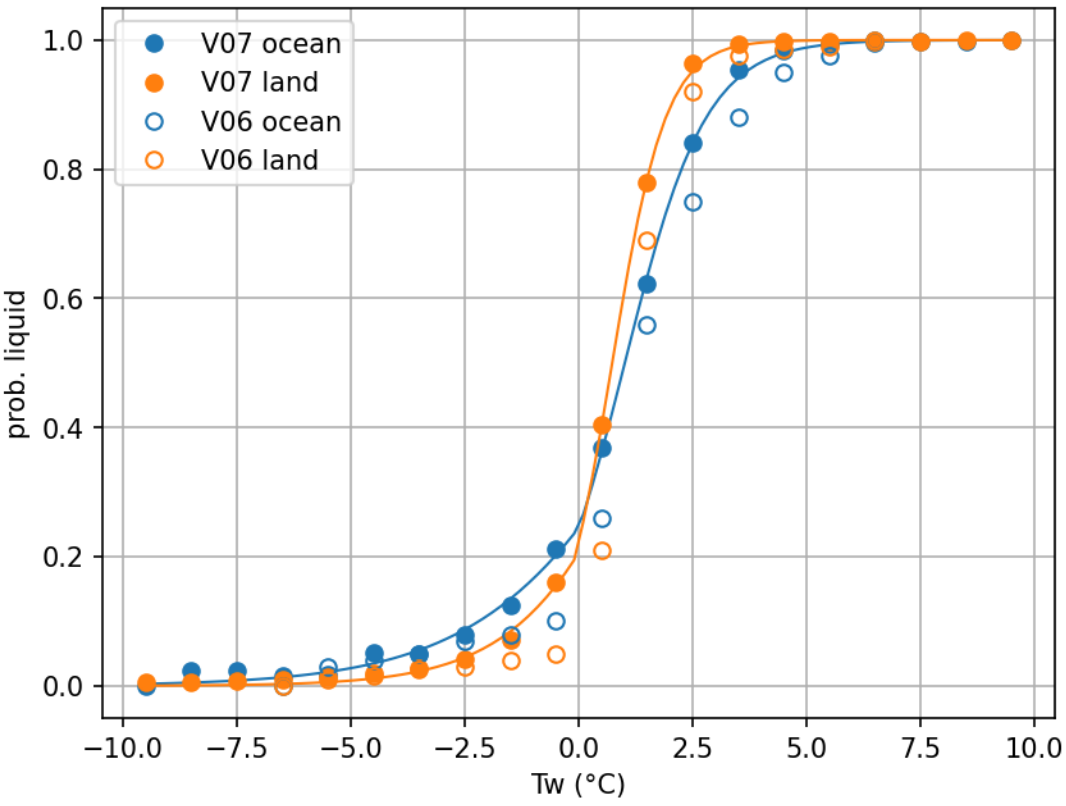

Figure 5: PLP as a function of T_w used in V07—obtained by fitting logistic functions to lookup tables recomputed using ERA5 variables—with the V06 values included for comparison.

At the monthly scale the PLP value could either be the fraction of the time that the precipitation is liquid or the fraction of the monthly accumulation that fell as liquid. The latter seems to be what most users will want, so this is the parameter computed. The monthly probability of liquid is the precipitation-rate-weighted average of all half-hourly probabilities in the month, except for grid boxes where zero precipitation is estimated for the month, in which case it is the simple average of all available probabilities in the month.

Note well that the assignment of phase does not change the units of precipitation, which is the depth of liquid. In the case of solid precipitation, this is usually referred to as snow water equivalent (SWE). The depth of fallen snow that corresponds to this SWE depends on the density of the snow. Typically, it takes about 10 mm of fallen snow to yield 1 mm of SWE, but the ratio depends on location, meteorological regime, time of year, and elevation. There is an excellent discussion of how Environment Canada is addressing this in Wang et al. (2017).

3.11 Error Estimates

Error estimates are a required item in the output datasets. The baseline fine-scale datasets errors are estimated following the TMPA downscaled monthly estimation scheme. The baseline monthly Final dataset error estimates are computed as part of the optimal estimation of the satellite-gauge combination. We expect that more sophisticated error fields will be incorporated as part of IMERG in the future, for example providing additional information on the error quantiles following Maggioni et al. (2014), Li et al. (2023), or the correlation parameter computed in the Kalman filter

methodology. In such a case, the critical problem is to limit the number of time/space-varying parameters that consequently require the insertion of additional parameter fields in each dataset.

3.12 Quality Index

Users have requested a "simple" quality index to give some guidance on when they should most trust IMERG. While the goal is reasonable, there is no agreement about how this quantity should be defined. After some discussion within the team, two distinctly different quality indices were chosen for the half-hourly and monthly data fields for implementation in V05 (and continued in V06 and V07), summarized below. It is a matter of investigation to determine if users find these insightful, or if different quality indices should be developed for future releases. Details are provided in the Appendix: IMERG V07 Quality Index.

3.12.1 QIh: Quality Index for Half-Hourly Data

At the half-hourly scale, the best metric is some measure of the relative skill that might be expected from the fluctuating mix of different passive microwave- and infrared-based precipitation estimates. The Kalman filter used in IMERG routinely recomputes estimates of correlation between GMI/TMI and each of the other satellite estimates in coarse blocks across the entire domain (90°N-S) and then uses these correlation coefficients to provide weights for use in the Kalman filter. However, the formalism of using correlations as weights does not provide an overall "merged correlation" for the combined estimate, so one approach is devised here.

The correlation coefficients developed for the Kalman filter are substituted for inverse error variance to compute the approximate correlation coefficient of the merged precipitation estimate. Furthermore, the correlation coefficients are transformed with the Fisher (1915) z-transformation before the computation and back-transformed afterwards, which is a simple variance stabilization transformation. This has the desirable property that combining two correlation values leads to a value that is higher than the original two, consistent with our expectation that the weighted average of two precipitation rates has higher skill than either of the original precipitation rates. Formally, the Fisher transformation requires that the two variables being correlated follow a bivariate normal distribution. While this is not true for precipitation, we adopt this approach as a first approximation to computing the correlation coefficient of the combined precipitation estimate because its use as a quality index seems reasonable and useful. The units are non-dimensional correlation coefficients.

One modification of the QI is its value over frozen surfaces. Now that PMW precipitation estimates are permitted over frozen surfaces in V07, the QI field is now extended to the poles. However, since the QI is based on regional correlation computed against GMI/TMI and then extrapolated to global coverage, this leads to unacceptably high values over the polar latitudes that do not reflect the actual (diminished) skill over frozen surfaces. Therefore, when calculating the QI value over frozen surfaces, the correlations are reduced by a factor depending on whether it is an imager or sounder and whether the grid box is over sea ice or snow-covered land. See Appendix: IMERG V07 Quality Index.

In summary, the half-hourly QI is a unitless number between 0 and 1. While it can be interpreted as the equivalent Pearson correlation coefficient of the precipitation estimate against GMI/TMI, it is best treated as a broad indicator of performance. Our internal evaluations show that the average skill increases with higher QI (though there is appreciable spread in this relationship). In particular, we recommend users further categorize the QI into three "stoplight" groups based on

its value: values below 0.5 are questionable, values above 0.75 are good, and the range 0.5 to 0.75 has fair quality. It is up to users to decide whether the lower quality data are acceptable for their particular application.

3.12.2 QIm: Quality Index for Monthly Data

At the monthly scale, a relatively well-founded metric exists for random error, based on Huffman's (1997) analysis of sampling error for a particular data source for a month. The general form of the relationship is simplified to a relationship that can be inverted to give the number of samples. When all the constants on the right-hand side are set for the gauge analysis, but final satellite-gauge values are used for the estimated precipitation and random error values, the number variable is defined as the equivalent number of gauges. Following Huffman (1997), the interpretation is that this is the approximate number of gauges required to produce the estimated random error, given the estimated precipitation. The units are gauges per area, and in the current implementation the area is carried as 2.5° × 2.5° of latitude/longitude, even though IMERG is computed on a much finer scale, in order to facilitate interpretation in large-error regions. Note that this formulation only addresses random error, not bias.

3.13 Algorithm Output

All output data files have multiple fields with PMM-mandated metadata and are written in HDF5, which is compatible with NetCDF4. All fields are produced for all data Runs. Table 5 lists the data fields. Recall that PMM provides an on-the-fly data subsetting by time, region, and parameter, so users are not required to download the entire file.

The output files for the various runs are identified with these prefixes (see *https://gpm.nasa.gov/sites/default/files/document_files/FileNamingConventionForPrecipitationProductsForGPMMissionV1.4.pdf*):

- 3B-HHR-E – half-hourly, Early Run
- 3B-HHR-L – half-hourly, Late Run
- 3B-HHR – half-hourly, Final Run
- 3B-MO – monthly, Final Run

As listed in Table 2, the notional requirement is that the output be on a global 0.1° grid. However, there is a strong argument that a fully global grid should be (approximately) equal-area, and this issue is under discussion within the project for future revisions. Also, the IR data are actually available on a 0.04° grid, and the question has been raised whether the notional grid size ought to be in the range 0.035°-0.05°. At present the baseline is left at 0.1° because there are scientific questions about downscaling PMW footprints to the finer scale, and operational questions about the resulting increased data volume.

3.14 Pre-Planned Product Improvements

Throughout the useful life of IMERG we plan for the code to be reasonably robust to errors, drop-outs, and changes in the make-up of the satellite constellation. The preceding discussion also detailed some developmental issues that are being addressed as we extend the IMERG record. In addition, the team considers it helpful to pre-plan certain enhancements to the code that we are fairly certain will be required at some point.

Table 5. Lists of data field variable names and definitions to be included in each of the IMERG output datasets. Primary fields of interest to users are in bold.

Half-hourly data file (Early, Late, Final)	
precipitation	**Multi-satellite precipitation estimate with gauge calibration (recommended for general use)**
precpitationUncal	Multi-satellite precipitation estimate
randomError	**Random error for gauge-calibrated multi-satellite precipitation**
MWprecipitation	Merged microwave-only precipitation estimate
MWprecipSource	Microwave satellite source identifier
MWobservationTime	Microwave satellite observation time
IRprecipitation	IR-only precipitation estimate
IRinfluence	Aggregate influence (in %) of the IR precipitation to the multi-satellite precipitation
probabilityLiquidPrecipitation	**Probability of liquid phase**
PrecipitationQualityIndex	**Quality Index for precipitation field**
Monthly data file (Final)	
precipitation	**Merged satellite-gauge precipitation estimate (recommended for general use)**
randomError	**Random error for merged satellite-gauge precipitation**
gaugeRelativeWeight	Weighting of gauge precipitation relative to the multi-satellite precipitation
probabilityLiquidPrecipitation	**Accumulation-weighted probability of liquid phase**
PrecipitationQualityIndex	**Quality Index for precipitation field**

Note well that *MWprecipitation* only includes microwave data (hence "MW"), meaning it has significant gaps. *precipitation* is the complete estimate that most users will want to access.

The index values for *MWprecipSource* are:

0 = no PMW observation	1 = TMI	2 = (unused)
3 = AMSR-2	4 = SSMI	5 = SSMIS
6 = AMSU	7 = MHS	8 = (unused)
9 = GMI	10 = (unused)	11 = ATMS
12 = AIRS	13 = TOVS	14 = CRIS
15 = AMSR-E	16 = SSMI F11	17 = Spare CSI 3
18 = Spare CSI 4	19 = Spare CSI 5	20 = SAPHIR (not used in V07)
21 = NOAA-21 ATMS	22 = Spare CTSS 3	23 = Spare CTSS 4
24 = Spare CTSS 5		

where CSI = conical-scanning imager and CTSS = cross-track-scanning sounder.

3.14.1 Add/Delete Input Data

Satellites come and go over time. For the most part, satellite dropouts, other than of the GPM Core itself, simply result in a smaller amount of input data for the system. Addition of data, on the other

hand, is potentially complicated by a range of possible priorities and calibration needs of the new sensor. In IMERG we follow the work pioneered in the Version 7 TMPA, where extra satellite slots are programmed in, separated into conical and cross-track scanners. When a new sensor comes on-line, it can be assigned to an appropriate-type slot and start contributing from that point forward, once the calibration coefficients are determined, which can require several months of data. However, including the new sensor's data record before the date/time on which it is instituted in the dataset requires retrospective processing (next Subsection).

3.14.2 Upgrade Input Data

When an existing sensor's data record is reprocessed, or a new sensor is introduced that has an archive not previously used, it is necessary to reprocess the archive of IMERG data to preserve consistent statistical behavior (to the extent possible) across the entire record. While reprocessing should not be undertaken lightly, given the computing demands on PPS and the disruption to the users, hard practical experience shows that we need to be more aggressive about this issue than had been the case previously for TMPA. For example, the second version of NESDIS AMSU, introduced in 2004, resulted in an underestimate of light rain. The result in TMPA during part of its Version 6 was a low bias in fractional coverage and rain amount over ocean. When an upgraded version of the NESDIS AMSU was introduced in early 2007 these biases were greatly reduced, but we allowed the inhomogeneity to persist in the Version 6 TMPA archive. As a result, users had to be continually reminded that the relatively low values are a known problem, a problem that was not fixed until the Version 7 TMPA reprocessing some five years later.

3.14.3 Polar Sensors

The Multi-Satellite team has extended IMERG to the polar regions, consistent with GPM's fully global focus. The first step was to add PMW snapshot estimates to the MW (called HQ up through V06) and merged data fields in V05, then we shifted to displacement vectors at higher latitudes by tracking TQV in MERRA-2 and GEOS FP. These vectors morph the available high-latitude precipitation estimates in the backward/forward Kalman filter to compute the output estimates. In a future version, we will consider adding available high-latitude estimates, including the leo-satellite AVHRR IR (and other channel) estimates. This development work will require close cooperation with the experts in high-latitude GV.

3.14.4 Near real-time Upgrades

It is likely that the near real-time products will require modifications to create the most useful output. For example, we started with somewhat loose latency limits for the Early and Late Runs and pared back the timing as we gained experience with the realities of the data reception. For the Late Run, this requires balancing the useful time range of backward-propagated microwave data against the latency of the following microwave overpass. If the daily gauge option is instituted for the Late Run, we believe we can fit it into the latency structure of the baseline scenario. That is, if the daily gauge analysis has a latency that is much longer than the Late Run satellites require, the daily gauge computation might be able to use calibration data up through the previous day.

3.14.5 Use Model Estimates

Validation work by Ebert et al. (2007) and Gehne et al. (2016) among others, demonstrates that numerical model estimates of precipitation can out-perform observational estimates at daily 0.25°x0.25° scale in the cool season over land. This stands in contrast to the poor performance by model estimates in tropical and subtropical conditions for day-to-day variations, diurnal cycle, and

seasonal variation. The Multi-Satellite team's experience in isolating bias in input datasets and the flexible, error-sensitive behavior of the Kalman filter concept seem to suggest that IMERG is a natural platform for testing the joint use of observational and model-based precipitation estimates. This is particularly true given that IMERG is now extended into polar regions (Sec. 3.14.3). It is absolutely clear that the team intends to maintain a robust observation-only capability throughout GPM to support a variety of applications, not the least being validation of model estimates. However, a parallel joint observation-model data field is a worthy contribution to the project and to advancing scientific understanding and societal benefit applications.

3.15 Processing Options

Since the clear mandate for the first IMERG algorithm was driven by a very aggressive schedule, the baseline algorithm was designed around code that was already running and tested. At the same time, the team had several concepts in research that might become sufficiently mature that one or more of them might be prime targets for upgrading the future versions.

3.15.1 Begin IMERG processing in January 1998

Even though the clear design goal in Table 2 is to start IMERG with 1 January 1998, Section 3.2.3 hints that IMERG currently starts in June 2000. This eventuates because the input CPC 4 km Merged Global IR data only become available in early February 2000, and we choose to wait until all accumulation files in the various calibrations are filled. Although we continue to hope that the remaining 25 months of CPC data will become available, an alternative is to use the GridSat archive of GEO-IR data (Knapp 2008). Such a move would require study, since GridSat data are provided on a subsampled 0.07° grid every 3 hours.

3.15.2 Use Multi-Spectral Geo-Data

Besides the thermal IR channel discussed above, geo-satellites also provide other channels, usually visible and one or more spread across the IR spectrum. Historically, these channels have not been used due to apparent modest improvements in skill, difficulties in handling the higher data volumes, and limitations to daylight hours (for visible). However, our ongoing dependence on geo-satellite data to fill large gaps between PMW overpasses and the increasing number of (non-microwave) channels on newer satellites make it important to reconsider this aspect. It is clear that multi-spectral GEO data provide important increases in skill using modern neural net approaches, particularly when visible data are used (e.g., Behrangi et al. 2009). Several important steps must be taken to capitalize on this apparent benefit in using multi-spectral data. First, the scientific development must be advanced to operational status. Second, we must work with the data providers to arrange for routine delivery of the data in a useful format, including a complete archive. Third, choices must be made on the selection of channels, recognizing that previous generations of geo-satellites had less-capable sensors than those now in use. The last two issues are being addressed by the GEO-Ring (Ken Knapp, personal communication) and ISCCP-NG (*https://cimss.ssec.wisc.edu/isccp-ng/*) projects, although it will likely take several years for these to be operational.

3.15.3 Incorporate Storm Development Information

Precipitation develops and decays over time periods that are short compared to the typical revisit time of the leo-PMW constellation. As noted above, the autocorrelation of observed and propagated precipitation fields may drop from 1.0 to ~0.6 within 30 minutes and further fall to ~0.4 or lower after an hour of propagation, while snapshot geo-IR precipitation estimates are

notoriously poor, but nonetheless provide a minimum floor of skill when a gridbox lacks recent propagated leo-PMW estimates. Taking a different approach, capturing the dynamic evolution of geo-IR cloud images may help to identify cloud systems in various stages of development. This approach to addressing the "cloud development problem" is a challenging area of research and requires further investigation to determine the best strategies for capturing the development process. One possibility is to drive a highly simplified conceptual cloud model with parameters computed from the geo-IR Tb data, as in the Bellerby et al. (2009) Lagrangian Model (LMODEL). Another is to modify the propagated leo-PMW precipitation estimates with time based on parameters computed from the geo-IR Tb data, as in the Behrangi et al. (2010) Rain Estimation using Forward Adjusted-advection of Microwave Estimates (REFAME).

3.15.4 Use Daily or Submonthly Gauges

The biases discussed previously vary on sub-monthly time scales, of course. To address this problem, we will examine the possibility of refining the bias correction approach described in Sec. 3.8 through the use of daily gauge analysis. The CHIMES scheme developed by Funk et al. (2022) with pentad accumulations of daily gauge data provides a strong candidate for using this data source. Alternatively, Xie et al. (2010) and Mega et al. (2019) have developed a technique to correct the bias in high-resolution satellite precipitation estimates through, respectively, matching the PDF of the satellite estimates against that of the daily gauge analysis and applying a cost function that balances temporal autocorrelation, climatological adjustment, and real-time gauge adjustment.

3.15.5 Improve Error Estimation

Error estimation has proved resistant to easy progress, in no small part because precipitation is a highly intermittent, non-negative process resulting in non-Gaussian, strongly skewed PDF's of precipitation events that are generated at very fine space and time scales, and which demonstrate multi-scale correlation structures. The current scheme for computing half-hourly random error estimates is based on the Huffman (1997) approach for monthly data, and badly needs to be replaced. The Precipitation Uncertainties for Satellite Hydrology (PUSH) scheme (Maggioni et al. 2014) seems to promise a clean computation of the full quantiles of precipitation for each grid box, which presumably encompasses both systematic and random error. Another promising concept is the Probabilistic QPE using Infrared Satellite Observations (PIRSO; Kirstetter et al. 2018). Despite the name, it should be applicable to IMERG. A third approach is outlined in Li et al. (2023). Note that none of these schemes directly addresses the grand challenge of accounting for the time/space error correlation structure in estimating error for arbitrary time/space averages of IMERG data.

4 TESTING

4.1 Algorithm Verification in the PPS System

As each generation of IMERG code is developed, it is validated on the development system. At the agreed-upon deliveries the entire package is assembled and transferred to PPS for integration and testing. This allows us to validate the PPS processing. The IMERG products are compared against coincident KF, PDIR, prior IMERG, and various ground validation fields. The goal in this stage is to shake out as many bugs and conceptual difficulties as possible, applying corrections to the production and near-real-time IMERG instantiations.

4.2 Algorithm Verification for the Different Runs

The main features to be validated between the near-real-time and production instantiations are the use of somewhat different input data sets and the addition of monthly gauge calibration in the Final run. As before, it is important to compare the results to the other estimates and validation data listed above.

4.3 Algorithm Validation

The more formal algorithm validation consists of examining various aspects of the IMERG results. At the snapshot level, comparison to the fine-scale NOAA Multi-Radar Multi-Sensor (MRMS) analyses, and to the PMM Kwajalein and GPM VN radar archives are considered key. As part of this effort, we carry out similar comparisons against the gridded Level 2 input data. The performance at larger space-time scales is assessed using accumulations of these datasets, as well as the CPC daily gauge analysis, the IPWG validation sites (Australia, CONUS, Japan, South America, Western Europe), the GPCC global monthly gauge analysis, the Pacific atoll data, and the ATLAS II buoy data. For higher-latitude validation, the GPCC data can be used to validate the satellite-only products. The team has access to Finnish Meteorological Institute precipitation gauge data, and to the Middleton Island NWS radar in the Gulf of Alaska (Watters et al. 2023). At a minimum, metrics include bias, root-mean-square error, mean absolute error, correlation, and skill scores. Decompositions into hit error, miss error, etc. following Tian et al. (2009) are considered as well. We are working with the validation teams to examine the IMERG datasets with the detailed validation approaches that they manage. Finally, we work with selected users, particularly hydrologists, to incorporate the test datasets and report their experiences to help determine what IMERG's level of skill is for their applications. Some early V07 results are displayed in the release notes, posted at

https://gpm.nasa.gov/sites/default/files/document_files/IMERG_V07_release_notes.pdf

and this discussion will be expanded as additional results are computed.

5 PRACTICAL CONSIDERATIONS

5.1 Module Dependencies

The baseline structure of IMERG is shown in Figure 2. We have not enforced consistency on the various boxes in the sense that some boxes might be programmed as multiple modules, while others will be computed in a single module. As summarized in Sec. 5.2, the data flow between modules, and between executions of the same module, is carried out using files, which typically have fixed names. Input and output datasets necessarily have names that reflect the time sequencing of the data that they contain.

5.1.1 Calibrations

The satellite-satellite calibrations, which include the PMW intercalibrations to a TRMM/GPM standard, IR-PMW precipitation calibration for the IR estimates, and the Kalman filter weights, are conceptually asynchronous with the actual half-hourly precipitation dataset processing. It is a matter of computational choice within PPS as to whether the calibrations are run sequentially or in parallel, but the system is designed to be very forgiving of occasional missed calibration match-ups – without significant loss of skill it can run with the then-current calibration files, as long as

the dropouts do not become too severe. For IMERG we necessarily run all the Early and Late calibrations on trailing accumulations of match-ups. The post-real-time Final run has to wait for the GPCC precipitation gauge analysis and the ECMWF ancillary data, so we accumulate the match-ups with a sufficient delay after real time that the Final calibrations are approximately centered, with the exception of the Kalman statistics, which consist of the current and previous two months of data.

The only important difference between near- and post-real-time runs comes in the last calibration, which is computed for the near-real-time as climatological adjustments based on the Final product, and for the post-real-time as calendar-month adjustments to, and combination with monthly gauge analyses. Note that in the previous V06 we did not do this last calibration, but it is being done in V07.

As noted above, we compute three runs of the algorithm, namely the "Early", "Late", and "Final" Runs at about 4 hr, 14 hr, and 3.5 months after observation time. The simplest approach is chosen, namely to maintain three entirely separate sets of files and to compute everything in each run. This eliminates dependencies between runs and facilitates retrospective processing.

5.1.2 Parallelization

The forward V05 retrospective processing revealed that the original KF propagated time series was programmed to be efficient in computational resources but required serial processing. This constituted significant impediment on a multi-processor server to timely completion for a long record. Thus, in V06 and subsequently V07 the forward propagated time series of PMW was re-worked to be computed from scratch for each half hour. Taking a cue from the backward propagation, which of necessity is recomputed anew for each half hour, the MW data in the previous 7 hours is used to develop the forward-propagated PMW field, since the KF correlations beyond 7 hours are negligible. While less efficient than the original scheme, the shift allows parallel computation for each half hour's forward propagation and significantly decreases wall clock time.

As well, the rotating accumulation files used for calibration impose a serial requirement. It is possible to have several "chunks" of years, each starting from scratch and just filling accumulation files until they are "full", then computing results. This would allow a coarse-scale parallelization that could reduce reprocessing wall clock time by a factor of the number of chunks (plus extra overhead).

5.2 Files Used in IMERG

Input, output, inter-module data transfer, and inter-run/static data storage is accomplished through files in IMERG. It is important to note that the granularity of the input data implies that two of each of the input types will have to be used in each half-hour with fair regularity. On the other hand, the precipitation gauge analysis provides only one file in a month, which is also true for the monthly Merged Satellite/Gauge product. Several of the options and planned upgrades will require the use, transport, and accumulation of data in additional files.

5.3 Built-In Quality Assurance and Diagnostics

To the extent possible, quality assurance checks are incorporated in the IMERG system. This includes quality checks of all input data, and of selected intermediate and output data based on

metrics developed for TRMM. The goal of these checks is to capture discrepancies before they propagate into the downstream processing. PPS toolkit warning and error messages are the primary mechanism used to flag potential problems. Optional diagnostic information is available to the operator when requested. It is possible that a separate, post-processing algorithm will be used to extend the quality assurance procedure to the Final product as part of the operational development. The goal of this post-processing algorithm would be to capture more subtle issues than observable during production.

5.4 Surface Temperature, Relative Humidity, and Pressure Data

The estimation of precipitation phase requires global surface temperature, relative humidity, and surface pressure data, since the operational algorithms cannot provide phase directly. The JMA model forecast analysis data are computed in 6-hour increments, and five 6-hour increments are provided within a single delivered file (i.e., a day). The data are provided in grib2 format, and converted to individual 6-hour files in flat binary by PPS using the standard wgrib2 utility. The ERA5 model data are available at 1-hour increments and converted from netCDF to binary. These binary files are read into IMERG and the appropriate parameters extracted and used to compute the percent probability of liquid phase.

5.5 Exception Handling

The IMERG system is designed to be robust in handling exceptions, including input file existence and integrity, command-line consistency, and routine data checks. It is the responsibility of the Multi-Satellite Team to create and update the toolkit error messages. When issues are flagged by the toolkit, additional diagnostic output has been integrated into the code by the developers to assist in isolating the problem when requested by the operator by setting the "debug" flag. Error reporting is used when exceptions are significant enough to halt execution. Warning reporting is used when exceptions should be noted, but processing can continue. In both cases, PPS contacts the algorithm developers to determine the severity of the exception and how best to address it.

5.6 Timing of Retrospective Processing for IMERG Products

As hinted in the previous Subsection, the decision to retrospectively process the IMERG archive as the result of algorithm changes in one or more input products critically depends on the availability of a completely reprocessed archive of the affected input product(s). In particular, when a general reprocessing is called for in the GPM suite of products, the IMERG products can be started only after the requisite Level 2 GPM products have been finalized and substantially reprocessed, allowing IMERG to apply the upgraded data for calibration and routine use in the products.

6 ASSUMPTIONS AND LIMITATIONS

6.1 Data Delivery

In general, the IMERG package is extremely forgiving of dropouts in individual sensors and inputs, including the calibrating sensor products, the geo-IR data, and the ERA5 reanalysis/numerical forecast data. Our experience with IMERG is that extended dropouts are rare for the GMI and DPR (and so CORRA-G), but extended dropouts have occurred for partner satellites and ancillary data. Typically, dropouts are the most likely in the Early Run due to the

stringent latency cut-off, less so for Late, and are frequently resolved by the time the Final is computed, but some fraction of the data indeed never is posted.

6.2 Assumed Sensor Performance

The implicit assumption in the IMERG code is that the various PMW datasets are either stable or unavailable. The main impact of data denial is on IMERG quality due to longer runs of morphed data and more-frequent use of IR estimates. What about changes in sensor performance? There is a time-dependent calibration update for the IR-PMW and GMI-CORRA calibrations in both near-real and post-real time. [For the TRMM era, all of the sensors were stable, including TMI.] So, if the IR or GMI is drifting, the time-dependent calibrations should account for the problem. However, using climatological GMI-to-other-PMW calibrations means a drifting GMI cannot be accommodated. We would be more flexible if we decide to routinely update these GMI-to-other-PMW calibrations, since drift in the GMI would be automatically accommodated, but such a modification would require a major development effort. For all sensors, including geo-IR and gauge, variations in the amount of unbiased noise should not automatically bias the results, although the resulting random errors will fluctuate correspondingly.

7 REFERENCES

Adler, R.F., G.J. Huffman, A. Chang, R. Ferraro, P. Xie, J. Janowiak, B. Rudolf, U. Schneider, S. Curtis, D. Bolvin, A. Gruber, J. Susskind, P. Arkin, E.J. Nelkin, 2003: The Version 2 Global Precipitation Climatology Project (GPCP) Monthly Precipitation Analysis (1979-Present). *J. Hydrometeor.*, **4**, 1147-1167, *doi:10.1175/1525-7541(2003)004<1147:TVGPCP>2.0.CO;2*

Behrangi, A., K. Hsu, B. Imam, S. Sorooshian, G.J. Huffman, R.J. Kuligowski, 2009: PERSIANN-MSA: A Precipitation Estimation Method from Satellite-based Multi-spectral Analysis. *J. Hydrometeor.*, **10**, 1414-1429, *doi:10.1175/2009JHM1139.1*

Behrangi, A., B. Imam, K. Hsu, S. Sorooshian, T.J. Bellerby, G.J. Huffman, 2010: REFAME: Rain Estimation Using Forward Adjusted-Advection of Microwave Estimates. *J. Hydrometeor.*, **11**, 1305-1321, *doi:10.1175/2010JHM1248.1*

Behrangi, A., G. Stephens, R.F. Adler, G.J. Huffman, B. Lambrigtsen, M. Lebsock 2014: An Update on Oceanic Precipitation Rate and Its Zonal Distribution in Light of Advanced Observations from Space. *J. Climate*, **27**, 3957-3965, *doi:10.1175/JCLI-D-13-00679.1*

Bellerby, T., K. Hsu, S. Sorooshian, 2009: LMODEL: A Satellite Precipitation Methodology Using Cloud Development Modeling. Part I: Algorithm Construction and Calibration. *J. Hydrometeor.*, **10**, 1081-1095, *doi:10.1175/2009jhm1091.1*

Bosilovich, M. G., R. Lucchesi, M. Suarez, 2016: MERRA-2: File Specification. GMAO Office Note No. 9 (Version 1.1), 73 pp, available from *https://gmao.gsfc.nasa.gov/pubs/docs/Bosilovich785.pdf*

Derin, Y., E. Anagnostou, A. Berne, M. Borga, B. Boudevillain, W. Buytaert, C.-H. Chang, H. Chen, G. Delrieu, Y.C. Hsu, W. Lavado-Casimiro, B. Manz, S. Moges, E.I. Nikolopoulos, D. Sahlu, F. Salerno, J.-P. Rodríguez-Sánchez, H.J. Vergara, K.K. Yilmaz, 2019: Evaluation of GPM-era Global Satellite Precipitation Products over Multiple Complex Terrain Regions. *Remote Sensing*, **11**, 2936, *doi.org:10.3390/rs11242936*

Ebert, E.E., J.E. Janowiak, C. Kidd, 2007: Comparison of Near-Real-Time Precipitation Estimates from Satellite Observations and Numerical Models. *Bull. Amer. Meteor. Soc.*, **88**, 47-64, *doi:10.1175/BAMS-88-1-47*

Ehsani, M.R., A. Behrangi, A. Adhikari, Y. Song, G.J. Huffman, R.F. Adler, D.T. Bolvin, E.J. Nelkin, 2021: Assessment of the Advanced Very High-Resolution Radiometer (AVHRR) for Snowfall Retrieval in High Latitudes Using CloudSat and Machine Learning. *J. Hydrometeor.*, **22**, 1591-1608, *doi:10.1175/JHM-D-20-0240.1*

Fuchs, T., J. Rapp, F. Rubel, B. Rudolf, 2001: Correction of Synoptic Precipitation Observations due to Systematic Measuring Errors with Special Regard to Precipitation Phases. *Phys. Chem. Earth (B)*, **26**, 689-693, *doi:10.1016/S1464-1909(01)00070-3*

Funk, C.C., P. Peterson, G.J. Huffman, M.F. Landsfeld, C. Peters-Lidard, F. Davenport, S. Shukla, S. Peterson, D.H. Pedreros, A.C. Ruane, C. Mutter, W. Turner, L. Harrison, A. Sonnier, J. Way-Henthorne, G.J. Husak, 2022: Introducing and evaluating the Climate Hazards center IMErg with Stations (CHIMES) - Timely Station-Enhanced Integrated Multi-satellitE Retrievals for Global Precipitation Measurement. *Bull. Amer. Meteor. Soc.*, **103**, E429–E454, *doi:10.1175/BAMS-D-20-0245.1*

Gehne, M., T.M. Hamill, G.N. Kiladis, K.E. Trenberth, 2016: Comparison of Global Precipitation Estimates across a Range of Temporal and Spatial Scales. *J. of Climate*, **29**, 7773-7795, *doi:10.1175/JCLI-D-15-0618.1*

Gelaro, R., W. McCarty, M.J. Suárez, R. Todling, A. Molod, L. Takacs, C.A. Randles, A. Darmenov, M.G. Bosilovich, R. Reichle, K. Wargan, L. Coy, R. Cullather, C. Draper, S. Akella, V. Buchard, A. Conaty, A.M. da Silva, W. Gu, G.-K. Kim, R. Koster, R. Lucchesi, D. Merkova, J.E. Nielsen, G. Partyka, S. Pawson, W. Putman, M. Rienecker, S.D. Schubert, M. Sienkiewicz, B Zhao, 2017: The Modern-Era Retrospective Analysis for Research and Applications, Version 2 (MERRA-2). *J. Climate.*, **30**, 5419–5454, *doi:10.1175/JCLI-D-16-0758.1*.

Hong, K.L. Hsu, S. Sorooshian, X. Gao, 2004: Precipitation Estimation from Remotely Sensed Imagery Using an Artificial Neural Network Cloud Classification System. *J. Appl. Meteorol.* **43**, 1834–1852, *doi:10.1175/JAM2173.1*

Huffman, G.J., R.F. Adler, D.T. Bolvin, G. Gu, E.J. Nelkin, K.P. Bowman, Y. Hong, E.F. Stocker, D.B. Wolff, 2007: The TRMM Multi-satellite Precipitation Analysis: Quasi-Global, Multi-Year, Combined-Sensor Precipitation Estimates at Fine Scale. *J. Hydrometeor.*, **8**, 38-55, *doi:10.1175/JHM560.1*

Huffman, G.J., R.F. Adler, A. Behrangi, D.T. Bolvin, E.J. Nelkin, G. Gu, M.R. Ehsani, 2023: The New Version 3.2 Global Precipitation Climatology Project (GPCP) Monthly and Daily Precipitation Products. *J. of Climate*, in revision.

Huffman, G.J., R.F. Adler, M. Morrissey, D.T. Bolvin, S. Curtis, R. Joyce, B McGavock, J. Susskind, 2001: Global Precipitation at One-Degree Daily Resolution from Multi-Satellite Observations. *J. Hydrometeor.,* **2**, 36-50, *doi:10.1175/1525-7541(2001)002<0036:GPAODD>2.0.CO;2*

Joyce, R.J., P. Xie, J.E. Janowiak, 2011: Kalman Filter Based CMORPH. *J. Hydrometeor.*, **12**, 1547-1563, *doi:10.1175/JHM-D-11-022.1*

Kirstetter, P.-E., N. Karbalaee, K. Hsu, Y. Hong, 2018: Probabilistic Precipitation Rate Estimates with Space-based Infrared Sensors. *Quart. J. Roy. Meteor. Soc.***,** **144**, 192-205, *doi:10.1002/qj.3243*

Knapp, K.R., 2008: Scientific Data Stewardship of International Satellite Cloud Climatology Project B1 Global Geostationary Observations. *J. Appl. Remote Sens.,* **2**, 023548, 21 pp. *doi:10.1117/1.3043461*

Krajewski, W.F., J.A. Smith, 1991: On the Estimation of Climatological Z–R Relationships. *J. Appl. Meteor.*, **30**, 1436–1445, *doi:10.1175/1520-0450(1991)030<1436:OTEOCR>2.0.CO;2*https://doi.org/10.1175/1520-0450(1991)030%3c1436:OTEOCR%3e2.0.CO;2

Legates, D.R., 1987: *A Cimatology of Global Precipitation Publications in Climatology*, **Vol. 40**, Univ. of Delaware, 85 pp.

Legates, D.R., C.J. Willmott, 1990: Mean Seasonal And Spatial Variability In Gauge-Corrected, Global Precipitation. *Internat. J. Climatol*., **10**, 111-127, *doi:10.1002/joc.3370100202*

https://gmao.gsfc.nasa.gov/products/documents/GEOS_5_FP_File_Specification_ON4v1_1.pdfLucchesi, R., 2018: File Specification for GEOS FP. GMAO Office Note No. 4 (Version 1.2), 61 pp, *https://gmao.gsfc.nasa.gov/pubs/docs/Lucchesi1203.pdf*

Li, Z., D.B. Wright, S.H. Hartke, D.B. Kirschbaum, S. Khan, V. Maggioni, P.-E. Kirstetter, 2023: Toward A Globally-Applicable UncertaintyQuantification Framework for Satellite MultisensorPrecipitation Products based on GPM DPR. *IEEE Trans. Geosci. Rem. Sens*., **61**, 4100415, 1-15, *doi:10.1109/TGRS.2023.3235270*

Maggioni, V., M.R.P. Sapiano, R.F. Adler, Y. Tian, G.J. Huffman, 2014: An Error Model for Uncertainty Quantification in High-Time Resolution Precipitation Products. *J. Hydrometeor*., **15**, 1274-1292, *doi:10.1175/JHM-D-13-0112.1*

Meng, H., B. Yan, R. Ferraro, C. Kongoli, 2012: Snowfall Rate Retrieval Using Passive Microwave Measurements. 12th Specialist Meeting on Microwave Radiometry and Remote Sensing of the Environment, 5-9 March 2012, Frascati, Italy.

Miller, J.R., 1972: A Climatological Z-R Relationship for Convective Storms in the Northern Great Plains. *15th Conf. on Radar Meteor.*, 153-154.

National Research Council. 2004: Climate Data Records from Environmental Satellites: Interim Report. Washington, DC: The National Academies Press, 150 pp, *doi:10.17226/10944*

Rajagopal, M., E. Zipser, G.J. Huffman, J. Russell, J. Tan, 2021: Comparisons of IMERG Version 06 Precipitation At and Between Passive Microwave Overpasses in the Tropics. *J. Hydrometeor*., **22**, 2117–2130, *doi:10.1175/JHM-D-20-0226.1*

Romanov, P., 2016: Global 4km Multisensor Automated Snow/Ice Map (GMASI) Algorithm Theoretical Basis Document. NOAA NESDIS Cent. for Sat. Appl. and Res., 61 pp, *http://www.star.nesdis.noaa.gov/smcd/emb/snow/documents/Global_Auto_Snow-Ice_4km_ATBD.pdf*

Schneider, U., A. Becker, P. Finger, A. Meyer-Christoffer, M. Ziese, B. Rudolf, 2014: GPCC's New Land-surface Precipitation Climatology based on Quality-controlled In-situ Data and its Role in Quantifying the Global Water Cycle. Theor. Appl. Climatol., 115, 15-40, *doi:10.1007/s00704-013-0860-x . http://link.springer.com/article/10.1007%2Fs00704-013-0860-x*

Schneider, U., P. Finger, A. Meyer-Christoffer, M. Ziese, A. Becker, 2018: Global Precipitation Analysis Products of the GPCC. GPCC Internet Publication, DWD, 17 pp, *ftp://ftp-anon.dwd.de/pub/data/gpcc/PDF/GPCC_intro_products_2008.pdf*.

Sevruk, B., 1989: Reliability of Precipitation Measurements. *Proc. WMO/IAHS/ETH Workshop on Precipitation Measurements*, St. Moritz, Switzerland, World Meteor. Org., 13–19.

Sims, E.M., and G. Liu, 2015: A Parameterization of the Probability of Snow–Rain Transition. *J. Hydrometeor*., **16**, 1466–1477, *doi:10.1175/JHM-D-14-0211.1*

Susskind, J., P. Piraino, L. Rokke, L. Iredell, A. Mehta, 1997: Characteristics of the TOVS Pathfinder Path A dataset. *Bull. Amer. Meteor. Soc.,* **78,** 1449–1472. *doi:10.1175/1520-0477(1997)078<1449:COTTPP>2.0.CO;2*

Tan, J., G. J. Huffman, D. T. Bolvin, and E. J. Nelkin, 2019: IMERG V06: Changes to the Morphing Algorithm. *J. Atmos. Oceanic Technol*., **36**, 2471–2482, *doi:10.1175/JTECH-D-19-0114.1*

Tan, J., G.J. Huffman, D.T. Bolvin, E.J. Nelkin, M. Rajagopal, 2021: SHARPEN: A Scheme to Restore the Distribution of Averaged Precipitation Fields. *J. Hydrometeor*., **22**, 2105–2116, *doi:10.1175/JHM-D-20-0225.1*

Tian, Y., C. Peters-Lidard, J. Eylander, R. Joyce, G. Huffman, R. Adler, K.-L. Hsu, F. J. Turk, M. Garcia, J. Zeng, 2009: Component Analysis of Errors in Satellite-Based Precipitation Estimates. *J. Geophys. Res, - Atmos*., **114**, D22104, *doi:10.1029/2009JD011949*

Turk, F.J., P. Arkin, E. Ebert, M. Sapiano, 2008: Evaluating High Resolution Precipitation Products. *Bull. Amer. Meteor. Soc*., **89**, 1911–1916, *doi:10.1175/2008BAMS2652.1*

Villarini, G., P.V. Mandapaka W.F. Krajewski, R.J. Moore, 2008: Rainfall and Sampling Errors: A Rain Gauge Perspective. *J. Geophys. Res*., **113**, D11102, *doi:10.1029/2007JD009214*.

Wang, X.L., H. Xu, B. Qian, Y. Feng, E. Mekis, 2017: Adjusted Daily Rainfall and Snowfall Data for Canada. *Atmos.-Ocean*, **55**, 155-168, *doi:10.1080/07055900.2017.1342163*

Watters, D.C., P.N. Gatlin, G.J. Huffman, P.E. Kirstetter, J. Tan, E.J. Nelkin, D.T. Bolvin, R. Joyce, D. Wolff, J. Wang, S. Ringerud, 2023; Oceanic Validation of IMERG Version 6 Precipitation using the GPM Validation Network. *J. Hydrometeor.*, submitted.

Xie, P., S.-H. Yoo, R. Joyce, Y. Yarosh, 2010: A High-Resolution Gauge-Satellite Merged Global Precipitation Analysis and Its Applications for Model Verifications. *WMO 3rd Internat. Conf. on QPE / QPF and Hydrol.*, 18-22 October, 2010, Nanjing, China.

You, Y., G. Huffman, V. Petkovic, L. Milani, J. X. Yang, A. Ebtehaj, S. Vahedizade, G. Gu, 2023: Evaluation of Snowfall Retrieval Performance of GPM Constellation Radiometers Relative to Spaceborne Radars. *J. Hydrometeor.*, **24**, 389–405, *doi:10.1175/JHM-D-22-0052.1*

You, Y., C. Peters-Lidard, S.J. Munchak, J. Tan, S. Braun, S. Ringerud, W. Blackwell, J.X. Yang, E. Nelkin, J. Dong, 2021: Improving Cross-Track Scanning Radiometers' Precipitation Retrieval over Ocean by Morphing. *J. Hydrometeor.*, **22**, 2393-2406, *doi:10.1175/JHM-D-21-0038.1*.

8 ACRONYMS

AIRS	Advanced Infrared Sounder
AMSR[E,-2,-3]	Advanced Microwave Scanning Radiometer [Earth Observing System, 2, 3]
ATBD	Algorithm Theoretical Basis Document
ATMS	Advanced Technology Microwave Sounder
AVHRR	Advanced Very High Resolution Radiometer
CLIMAT	Monthly Climatological Data
CONUS	CONtiguous U.S.
CORRA[-G,-T]	Combined Radar-Radiometer Algorithm [specifically for GPM, TRMM]
CPC	Climate Prediction Center
CPO	Climate Program Office

CrIS	Cross-track Infrared Sounder
CRU	Climate Research Unit
DISC	Data and Information Services Center
DMSP	Defense Meteorological Satellite Program
DPR	Dual-frequency Precipitation Radar
DWD	Deutscher Wetterdienst
ECMWF	European Centre for Medium-range Weather Forecasting
ERA5	ECMWF Reanalysis version 5
EUMETSAT	European organization for the exploitation of Meteorological Satellites
FAO	Food and Agriculture Organization
GCOMW	Global Change Observation Mission - Water
geo	geosynchronous Earth orbit
GEO-Ring	GEO constellation Ring
GEOS-5	Goddard Earth Observing System model, Version 5
GEOS FP	Goddard Earth Observing System Forward Processing
GES DISC	Goddard Earth Science Data and Information System Center
GIOVANNI	Geospatial Interactive Online Visualization ANd aNalysis Infrastructure
GEWEX	Global Energy and Water cycle Experiment
GHCN	Global Historical Climatology Network
GMI	GPM Microwave Imager
GMS	Geosynchronous Meteorological Satellite
GOES	Geosynchronous Operational Environmental Satellite
GOSAT	Greenhouse gases Observing SATellite
GPCC	Global Precipitation Climatology Centre
GPCP	Global Precipitation Climatology Project
GPM	Global Precipitation Measurement mission
GSFC	Goddard Space Flight Center
G-WADI	Water and Development Information for Arid Lands – a Global Network
HDF	Hierarchical Data Format
IMERG	Integrated Multi-satellitE Retrievals for GPM
IR	Infrared
ISCCP-NG	International Satellite Cloud Climatology Project – Next Generation
JMA	Japanese Meteorological Agency
JPSS	Joint Polar Satellite System
KF	Kalman filter version
leo	low Earth orbit
LMODEL	Lagrangian Model
LT	Local Time
MERRA-2	Modern-Era Retrospective analysis for Research and Applications, Version 2
METOP[-SG]	Meteorological Polar Orbit satellite [Second Generation]
MHS	Microwave Humidity Sounder
MIS	Microwave Imager Sensor
MRMS	(NOAA) Multi-Radar Multi-Sensor (precipitation analysis)
MTSat	Multi-functional Transport Satellite
MWI	Microwave Imager
MWS	Microwave Sounder

NASA	National Aeronautics and Space Administration
NCEI	National Centers for Environmental Information (formerly NCDC)
NESDIS	National Environmental Satellite Data and Information Service
NetCDF	Network Common Data Format
NEWS	NASA Energy and Water Studies program
NOAA	National Oceanic and Atmospheric Administration
NRT	Near Real Time
NSF	National Science Foundation
PDF	Probability Density Function
PDIR	PERSIANN – Dynamic Infrared-Rain Rate
PERSIANN	Precipitation Estimation from Remotely Sensed Information using Artificial Neural Networks
PERSIANN-CCS	PERSIANN–Cloud Classification System
PERSIANN-CDR	PERSIANN–Climate Data Record
PLP	Probability of Liquid Phase
PMM	Precipitation Measurement Missions
PMW	Passive Microwave
PPS	Precipitation Processing System
PR	Precipitation Radar
PRECTOT	Total precipitation from atm model physics (surface precipitation rate)
REFAME	Rain Estimation using Forward Adjusted-advection of Microwave Estimates
RT	Real Time
SAHRA	Sustainability of semi-Arid Hydrology and Riparian Areas
SNPP	Suomi National Polar-orbiting Partnership
SSMI	Special Sensor Microwave Imager
SSMIS	Special Sensor Microwave Imager/Sounder
SYNOP	Synoptic Weather Report
TCI	TRMM Combined Instrument product
TMI	TRMM Microwave Imager
TMPA	TRMM Multi-satellite Precipitation Analysis
TQL	Total precipitable liquid water
TQV	Total precipitable water vapor
TRMM	Tropical Rainfall Measuring Mission
UNESCO	United Nations Educational Scientific and Cultural Organization
URL	Universal Resource Locator (usually the web address)
USWRP	U.S. Weather Research Program
UTC	Universal Coordinated Time
Version 6, 7, 8	TRMM version numbers (note well the single digit)
V03, V04, V05, V06, V07	GPM version numbers (note well the leading zero digit)
WSF-M	(DoD) Weather Satellite Follow-on - Microwave
3B-HHR-E	half-hourly gridded precipitation estimate, Early Run
3B-HHR-L	half-hourly gridded precipitation estimate, Late Run
3B-HHR	half-hourly gridded precipitation estimate, Final Run
3B-MO	monthly gridded precipitation estimate, Final Run

9 APPENDIX: IMERG V07 QUALITY INDEX

9.1 Summary

Users have requested a "simple" quality index (QI) to give some guidance on the degree to which they should trust the Integrated Multi-satellitE Retrievals for GPM (IMERG). While the goal is reasonable, there is no agreement about how this quantity should be defined. After some discussion within the team, two distinctly different quality indices were chosen for the half-hourly and monthly data fields (QIh and QIm, respectively) for implementation in V05 and further refined in V06 and V07. Effectively, QIh is related to the Pearson correlation coefficient of the precipitation estimate against GMI/TMI and the QIm can be interpreted as the equivalent number of gauges in a monthly gauge analysis at 2.5° × 2.5° that correspond to the precipitation and precipitation error estimates in the grid box, though both metrics are intended to be used as a relative measure of skill.

In V07, the major changes in the algorithm that affect QIh are: upgrades to the passive microwave (PMW) and infrared (IR) precipitation algorithms, the inclusion of instantaneous PMW estimates in the Kalman filter, and the treatment of estimates over frozen surfaces. The latter two changes are elaborated below. QIm is unchanged in V07. As with previous versions, we welcome feedback and suggestions about how the QI can be improved.

9.2 QIh: Quality Index for Half-Hourly Data

At the half-hourly scale, we choose a metric that estimates the skill that might be expected from the fluctuating mix of different PMW- and IR-based precipitation estimates. The Kalman filter used in IMERG (and originated in the CPC KF-CMORPH algorithm, Joyce et al. 2011) routinely updates regional Pearson correlation coefficients (or "correlations" hereafter) between GMI/TMI and each of the other satellite estimates, and then uses these correlations (squared) to provide weights for use in the combination of instantaneous PMW, forward-propagated PMW, backward-propagated PMW, and IR precipitation estimates. Specifically, the correlations are computed for each half-hour forward and backward "time step" away from the current half hour, separately for imager and sounder estimates. For example, if a grid box has an instantaneous AMSR2 estimate (correlation 0.8), a 90-min forward propagated SSMIS estimate (correlation 0.4), and a 60-min backward propagated MHS estimate (correlation 0.3), the Kalman filter estimate would be an average of all three estimates with relative weights 0.8^2, 0.4^2, and 0.3^2 respectively.

How should these Kalman correlation values be combined into a half-hourly QI? There is no formalism for computing an overall correlation, but there are two conditions that we impose. First, the combined value should fall within the range of 0 to 1 so as to retain its interpretation as a correlation-based value. This rules out a simple sum of the correlation values (which in the example above would result in a value of 1.5). Second, the combined value should have a value higher than each of the inputs, consistent with our expectation that each input incrementally improves—even if only slightly—the quality of the final estimate. This eliminates the mean of the correlation values (which in the example above would result in a value of 0.5) as an option. Based on these two conditions, we devised the following.

The usual approach to compute the root mean square error of a combined estimate (σ_t) from the individual root mean square error estimates (σ_a and σ_b):

$$\sigma_t = \frac{\sigma_a \sigma_b}{\sqrt{\sigma_a^2 + \sigma_b^2}} \quad (1)$$

The Kalman filter initially developed at CPC as part of CMORPH and adopted in IMERG uses squared correlation (c^2) in place of $1/\sigma^2$ in the weighting of the input precipitation estimates, so substituting $1/c$ for σ in (1) and simplifying,

$$c_t = \sqrt{c_a^2 + c_b^2}\,, \quad (2)$$

where c_a and c_b are individual correlations for estimates a and b, and c_t is the estimated correlation for the combination of estimates a and b.

This formulation has the advantage of producing correlations higher than the individual input terms—satisfying the second condition—highest when c_a and c_b are equal, and declining to c_a as c_b goes to zero (and vice-versa). However, if both c's are close to 1, the resulting c_t can exceed 1 and be as high as 1.414, violating the first condition. One solution to this quandary is to introduce a variance-stabilizing transformation, and one simple choice is the Fisher (1915) z-transformation,

$$z = \operatorname{arctanh}(c)\,, \quad (3)$$

The transformed value z takes on large values as c approaches 1 (or −1), so transforming to z, performing calculations with z, and back-transforming satisfies both conditions. That is, if instead of (2), we have

$$z_t = \sqrt{z_a^2 + z_b^2}\,, \quad (4)$$

we can combine (3) and (4) to get

$$c_t = \tanh\left(\sqrt{\operatorname{arctanh}^2(c_a) + \operatorname{arctanh}^2(c_b)}\right). \quad (5)$$

Formally, the Fisher z-transformation requires that the two variables being correlated follow a bivariate normal distribution. While this is not true for precipitation, we adopt this approach as a first approximation to computing the correlation of the combined precipitation estimate because its use as a QIh seems reasonable and useful. With the multiple inputs in IMERG, the equation becomes

$$c_t = \tanh\left(\sqrt{\operatorname{arctanh}^2(c_{mw}) + \operatorname{arctanh}^2(c_{fp}) + \operatorname{arctanh}^2(c_{bp}) + \operatorname{arctanh}^2(c_{ir})}\right), \quad (6)$$

where c_{mw} is the instantaneous PMW estimate correlation, c_{fp} is the forward-propagated PMW estimate correlation, c_{bp} is the backward-propagated PMW estimate correlation, and c_{ir} is the IR estimate correlation. Note that IR estimates are only included when there is no PMW estimate within ±30 minutes from the current half-hour, so in practice there are at most three inputs as there is never simultaneously an instantaneous PMW estimate and an IR estimate. The inclusion of the instantaneous PMW estimate in the Kalman filter is a new development in V07; whereas previously such estimates were directly used as the final satellite-only field with its correlation value as the QIh, its inclusion in the Kalman filter would result in a higher QIh value, consistent with the second condition.

The way in which the PMW field is handled in the current implementation of IMERG prevents calculating the "t = 0 h" correlations between the instantaneous PMW estimates and GMI/TMI in the Kalman filter. Therefore, we need an approximate value. Lacking strong justification for alternatives, we approximate the "t = 0 h" correlations by first computing a set of monthly baseline correlations from gridded and intercalibrated PMW estimates from December 2014 to November 2015, then include them into the Kalman correlations with dynamic adjustments based on the adjacent "t = ±0.5 h" correlations (i.e., correlations against GMI/TMI of the PMW estimates propagated forward and backward in time by one half-hour).

One complicating factor in V07 is the implementation of the Scheme for the Histogram Adjustment of Ranked Precipitation Estimates in the Neighborhood (SHARPEN). Implemented after the Kalman filter module, SHARPEN replaces the averaged precipitation value from the Kalman filter with a value selected from the parent fields in the vicinity of the grid box, effectively shuffling the precipitation rates around the region. This introduces complications to the interpretation of QIh. On the one hand, the precipitation rate in a grid box is no longer directly associated with the QIh value in that grid box; on the other hand, the Kalman filter precipitation rate with which the QIh value is associated still asserts its influence by determining its rank in SHARPEN. This posed a dilemma for us: do we shuffle the QIh value alongside the precipitation value, or do we keep the QIh value as is? For simplicity, we adopt the latter approach, leaving the QIh value untouched by SHARPEN, and urge users to be aware of this complication.

A special adjustment to the QIh relates to estimates over frozen surfaces. Traditionally, PMW retrievals struggled over frozen surfaces due to the difficulty in distinguishing the surface-based scattering from the scattering signal of frozen hydrometeors aloft. Thus, up to V06, we have made the decision to mask such estimates (including propagated precipitation), resulting in the use of IR estimates within 60°N-S and missing values poleward. In V07, we deem the GPROF PMW algorithm sufficiently advanced to lift this longstanding rule masking out frozen surface. However, since the QIh is based on regional correlation computed against GMI/TMI (covering the latitude bands ±65/35°) and then extrapolated to global coverage, this leads to unacceptably high values over the polar latitudes that do not reflect the diminished skill from which GPROF estimates still suffer. Therefore, over frozen surfaces, the correlations used in calculating the QIh value are reduced by a multiplicative factor depending on whether the sensor is an imager or sounder, and whether the grid box is over sea ice or frozen land (as indicated by the daily NOAA Autosnow product). Specifically, this factor is 0.112 for imagers and 0.275 for sounders over frozen land, and 0.495 for imagers and 0.282 for sounders over sea ice. These four factors are estimated by comparing a sample of the Kalman correlations of instantaneous PMW estimates with correlations computed against KuPR by You et al. (2023).

Lastly, there are rare occasions in which the QIh value is set to zero. This occurs when all four possible inputs into the Kalman filter are missing. This is extremely rare as it requires extended data dropouts in the inputs, which is more likely earlier in the record when the PMW constellation is smaller. When such a situation occurs, we decided that having a precipitation value, however inaccurate, is preferable to most users over having no value, so IMERG will simply select a precipitation rate from the IR field within ±12 h and flag it by assigning zero to the QIh value. Of course, this only works in the IR coverage area of 60°N-S; at higher latitudes the values are left at "missing".

The c_t as defined in (6) with the approximations and adjustments described above is adopted as QIh.

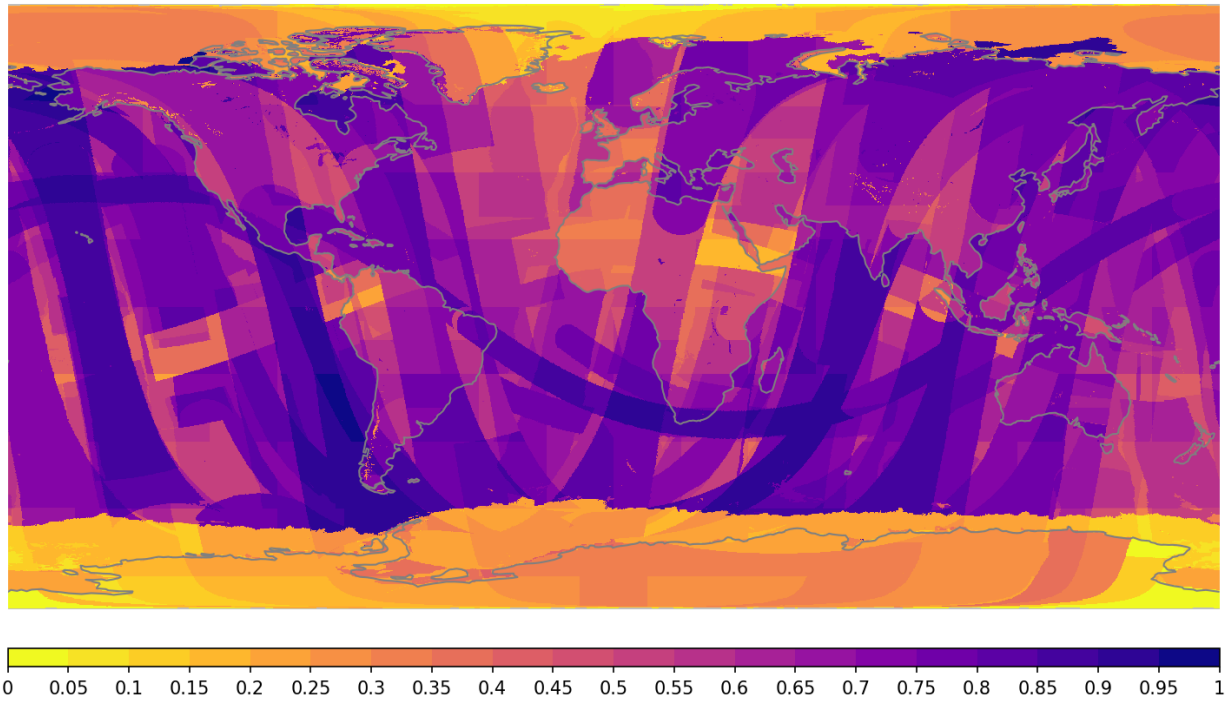

Figure 6: QI for the half-hourly IMERG Final Run for the period 0000–0030 UTC on 1 July 2014. The QIh value is related to the expected correlation of the precipitation estimate against GMI/TMI.

9.3 Advice on Using the Half-Hourly Quality Index

An example of QIh for the IMERG Final Run is shown in Figure 6. There are several salient features in the QIh field. First, the field has a pattern that reflects the low-Earth orbit swaths of the PMW sensors, indicating the drop in skill of estimates further in time from an overpass. Second, there are large regional blocks as well as land-ocean differences, reflecting how the Kalman correlations are computed. Third, the values at high latitudes have diminished values, caused by the adjustment over frozen surfaces.

Our evaluation of the IMERG V07 precipitation estimates against the Multi-Radar Multi-Sensor product specially processed for GPM Ground Validation (GV-MRMS; Kirstetter et al. 2014) reveals that the skill of the precipitation estimates has a modest to moderate dependence on the QIh value (Figure 7). Specifically, metrics that reflect the systematic error, such as bias, show a slight

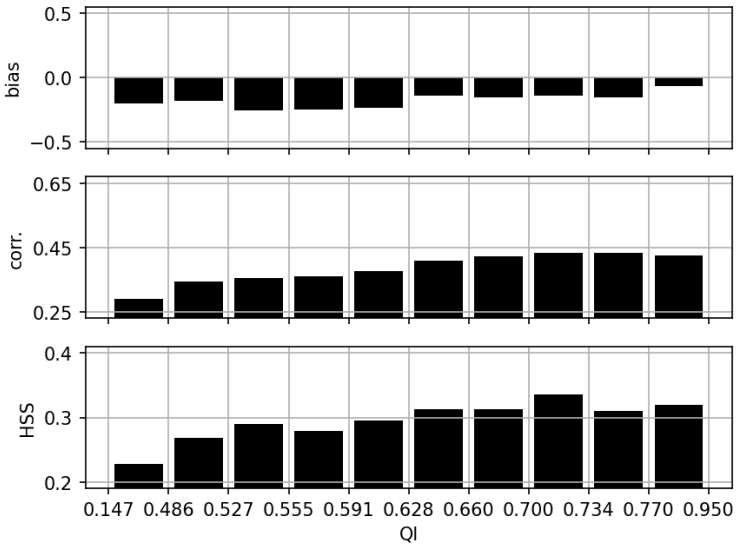

Figure 7: Evaluation of the precipitation estimates against GV-MRMS as a function of different QI percentile bins for July 2014.

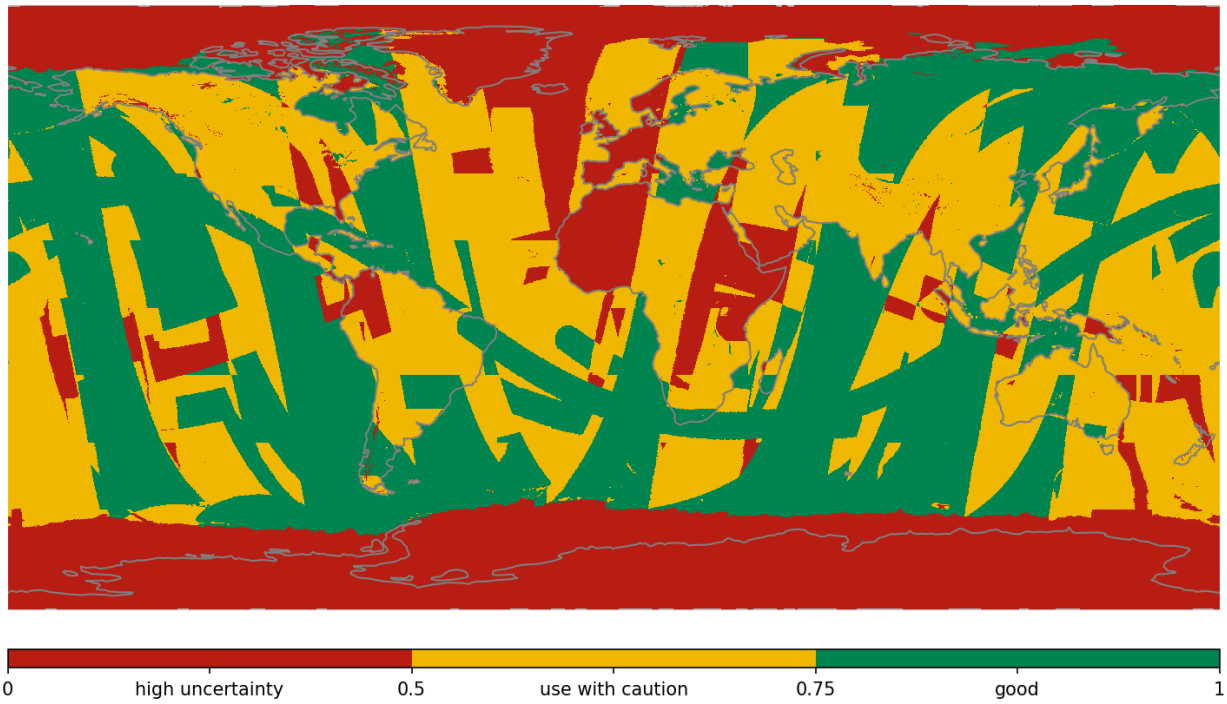

Figure 8: A simplification of Figure 6 (QIh) into a three-class "stoplight" grouping.

improvement with increasing QIh, whereas metrics that reflect the random error, such as correlation and HSS, show a moderate improvement with increasing QIh. Therefore, QIh does provide a general indication of the skill of the precipitation estimates. However, we expect that—as always with precipitation—there is substantial variability in this relation, so it should not be assumed that a precipitation estimate with a higher QIh is *always* more accurate than a precipitation estimate with a lower QIh, as should be apparent in the non-monotonic relationship in Figure 7.

To address the "simple index" goal for QIh, we recommend the following three-class "stoplight" grouping on the basis of a reasonable distribution of all three classes within ±60°N/S:

$0 \leq \text{QIh} < 0.5$: "red", high uncertainty in the precipitation estimate
$0.5 \leq \text{QIh} < 0.75$: "yellow", use precipitation estimate with caution
$0.75 \leq \text{QIh} \leq 1$: "green", precipitation estimate is of good skill

Figure 8 shows the simplification of the particular half-hourly QIh field in Figure 6 into these three "stoplight" classes.

Finally, we would like to remark on the "so what?" question associated with QIh; namely, if a precipitation estimate is classified as "red", what estimate should the user use instead? This is a question that only the user can answer depending on their application. If the application can tolerate some missing information or have alternative sources of precipitation estimates, then the user can choose to discard precipitation estimates of high uncertainty, though they should be aware that this may introduce diurnal sampling bias given the sun-synchronous orbits of most of the satellites. If the application requires complete sampling, then perhaps having low quality data is better than no data at all. We provide the QIh as information on the reliability of the precipitation estimate, and it is up to the user to use this information in a way that is relevant to their application.

9.4 QIm: Quality Index for Monthly Data

At the monthly scale, a relatively well-founded metric exists for random error, based on Huffman's (1997) analysis of sampling error for a particular data source for a month. The general form of the relationship is

$$\sigma_r^2 = \frac{\bar{r}^2}{N_I}\left(\frac{H}{p} - 1\right), \tag{7}$$

where σ_r is random error, $\bar{r}$ is the time-average of the precipitation rate samples, N_I is the number of independent samples in $\bar{r}$, H is the non-dimensional second moment of the probability distribution of the precipitation rates, and p is the frequency of all nonzero precipitation. Huffman (1997) proceeds to simplify (6) to the approximate expression

$$\sigma_r^2 \cong \frac{H}{I}\frac{(\bar{r} + S)}{N}\left[24 + 49\sqrt{\bar{r}}\right], \tag{8}$$

where $\bar{r}$ and N are available for each grid box in the monthly estimate, I is a multiplicative constant expressing the fraction of N that is "independent", and H/I and S are global constants that are approximated with validation data for each sensor type. This relationship is simple enough that it can be inverted for N. When all the constants are set for the gauge analysis, but the $\bar{r}$ and σ_r^2 used are the final satellite-gauge precipitation estimate and random error variance,

$$N \cong \left(\frac{H}{I}\right)_g \frac{\left(\bar{r} + S_g\right)}{\sigma_r^2}\left[24 + 49\sqrt{\bar{r}}\right], \tag{9}$$

and this special N is defined as the equivalent number of gauges. Following Huffman (1997), the interpretation is that this is the approximate number of gauges required to produce the estimated

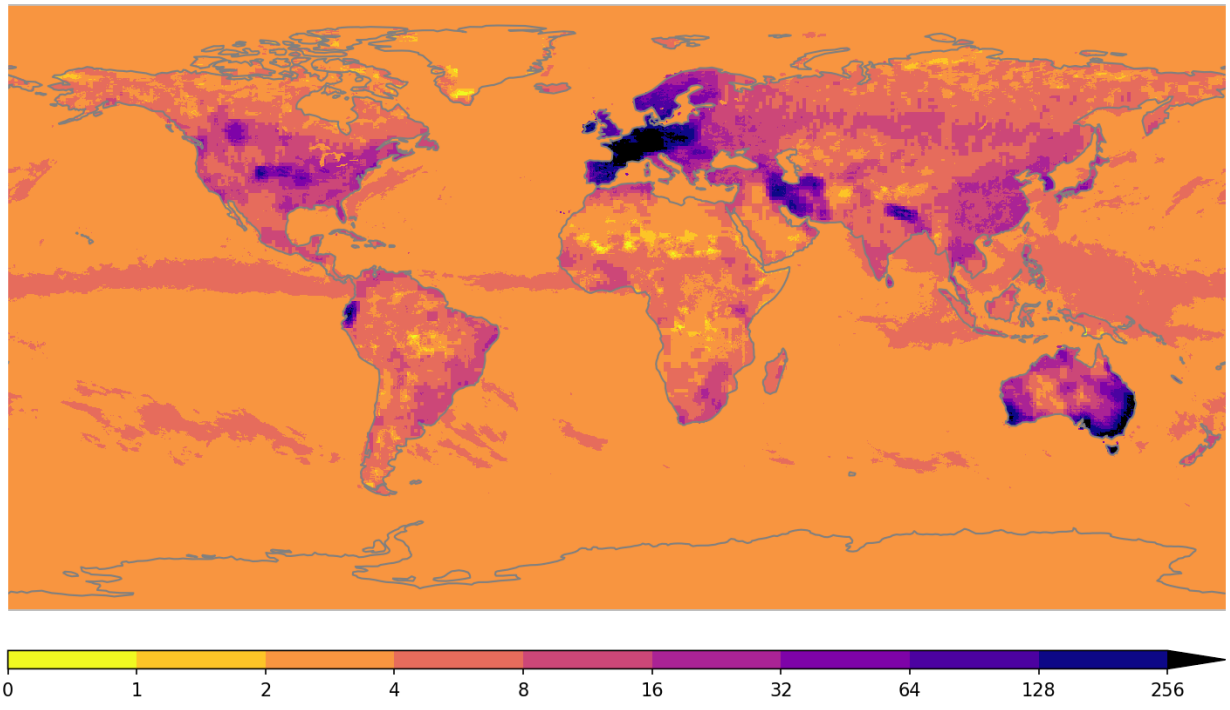

Figure 9: QI for the monthly IMERG Final Run for July 2014. The QIm value can be interpreted as the number of equivalent gauges per 2.5° × 2.5° box.

random error, given the estimated precipitation. The units are gauges per area, and in the current implementation the area is carried as 2.5° × 2.5° of latitude/longitude, even though IMERG is computed on a much finer scale, in order to facilitate interpretation in large-error regions.

In V07, this definition based on (9) for QIm is unchanged. We considered making adjustments to QIm over frozen surfaces similar to those for QIh, but elected not to for two reasons. First, as is evident from Figure 9, the monthly QI is less a function of the PMW sensor and more a function of the gauge coverage. The reason for the QIh adjustment based on frozen surface coverage is the expected diminished performance of PMW sensors (and possibly IR sensors too) as well as the reference of GMI/TMI, one that in theory is not strongly relevant here. Second, the gauge error estimation is based on rainfall, whereas precipitation over frozen surfaces tends to be snowfall, which likely drives higher errors for the gauges. Since it is unclear how any adjustments can be made, we elect not to adjust QIm over frozen surfaces (or frozen precipitation) in V07 and urge users to be aware of the ambiguous interpretation. This issue deserves attention in preparation for V08.

N, the equivalent number of gauges, is adopted as QIm. Note that *N* is dominated by the number of gauges except where gauges are sparse.

9.5 Advice on Using the Monthly Quality Index

An example of QIm for the IMERG Final Run is shown in Figure 9. [Recall that monthly data are computed explicitly in the Final Run, but not the Early or Late Runs.] Over oceans, the equivalent gauges metric largely tames the variation of random error with precipitation rate as the sampling by the satellite estimates is relatively uniform. Over land, QIm largely reflects the distribution of precipitation gauges, except it has the lower limit of the satellite equivalent gauges (similar to the

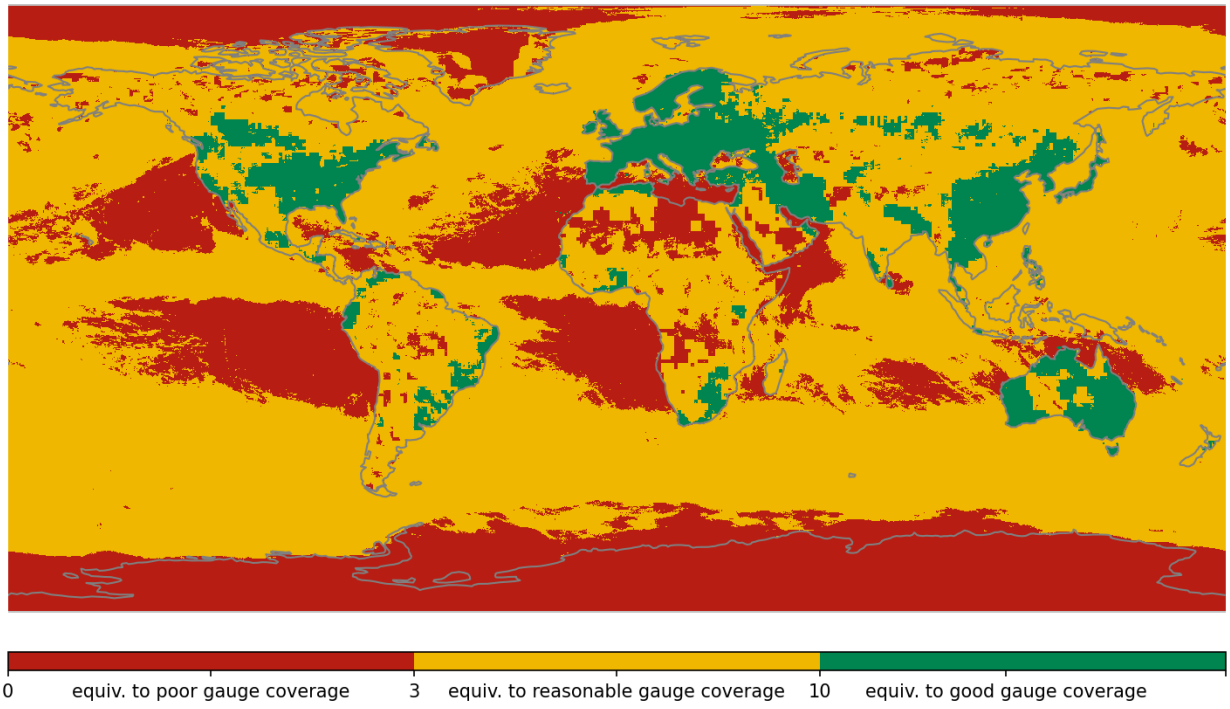

Figure 10: A simplification of Figure 9 (QIm) into a three-class "stoplight" grouping.

values over ocean) where gauges are extremely sparse. The QIm values outside 60°N-S reflect relatively sparse gauges (over snowy/icy land) and PMW sampling over ice-free ocean and land.

QIm has a longer history at the 2.5° scale, but is relatively new for the 0.1° scale. Based on experience with regions with different QIm values, the advice on "stoplight" values is:

$0 \leq \text{QIm} < 3$: "red", equivalent to regions with poor gauge coverage
$3 \leq \text{QIm} < 10$: "yellow", equivalent to regions with enough gauge data for reasonable bias adjustment, but still routinely requiring interpolation to fill in gaps between stations
$10 \leq \text{QIm}$: "green", equivalent to regions with good-to-excellent gauge networks

Just as with QIh, these ranges are selected to give a reasonable distribution of all three classes. Figure 10 shows the simplification of the QIm field in Figure 9 into these three "stoplight" classes.

9.6 References

Fisher, R.A., 1915: Frequency Distribution of the Values of the Correlation Coefficient in Samples of an Indefinitely Large Population. *Biometrika*, **10**, 507–521. *doi:10.2307/2331838*

Huffman, G.J., R.F. Adler, D.T. Bolvin, G. Gu, E.J. Nelkin, K.P. Bowman, Y. Hong, E.F. Stocker, D.B. Wolff, 2007: The TRMM Multi-satellite Precipitation Analysis: Quasi-Global, Multi-Year, Combined-Sensor Precipitation Estimates at Fine Scale. *J. Hydrometeor.*, **8**, 38-55. *doi:10.1175/JHM560.1*

Joyce, R.J., P. Xie, J.E. Janowiak, 2011: Kalman Filter Based CMORPH. J. Hydrometeor., 12, 1547-1563. *doi:10.1175/JHM-D-11-022.1*

Kirstetter, P.-E., Y. Hong, J. J. Gourley, Q. Cao, M. Schwaller, and W. Petersen, 2014: Research Framework to Bridge from the Global Precipitation Measurement Mission Core Satellite to the Constellation Sensors Using Ground-Radar-Based National Mosaic QPE. *Remote Sensing of the Terrestrial Water Cycle, Geophys. Monogr.*, Vol. 206, Amer. Geophys. Union, 61–79. *doi:10.1002/9781118872086.ch4*

You, Y., G.J. Huffman, V. Petkovic, L. Milani, J. X. Yang, A. Ebtehaj, S. Vahedizade, G. Gu, 2023: Evaluation of Snowfall Retrieval Performance of GPM Constellation Radiometers Relative to Spaceborne Radars. *J. Hydrometeor.*, **24**, 389–405. *doi:10.1175/JHM-D-22-0052.1*